Projecting end of century climate extremes and their impacts on the hydrology of a representative California watershed

Fadji Z. Maina[1,3*], Alan Rhoades[2], Erica R. Siirila-Woodburn[1], Peter-James Dennedy-Frank[1]

[1] Energy Geosciences Division, Lawrence Berkeley National Laboratory 1 Cyclotron Road, M.S. 74R-316C, Berkeley, CA 94704, USA

[2] Climate and Ecosystem Sciences Division, Lawrence Berkeley National Laboratory 1 Cyclotron Road, M.S. 74R-316C, Berkeley, CA 94704, USA

[3] now at NASA Goddard Space Flight Center, Hydrological Sciences Laboratory, Greenbelt, MD, USA

*Corresponding Author: fadjizaouna.maina@nasa.gov

Abstract

In California, it is essential to understand the evolution of water resources in response to a changing climate to sustain its economy and agriculture and to build resilient communities. Although extreme conditions have characterized the historical hydroclimate of California, climate change will likely intensify hydroclimatic extremes by the End of Century (EoC). However, few studies have investigated the impacts of EoC extremes on watershed hydrology. We use cutting-edge global climate and integrated hydrologic models to simulate EoC extremes and their effects on the water-energy balance. We assess the impacts of projected driest, median, and wettest water years under a Representative Concentration Pathway (RCP) 8.5 on the hydrodynamics of the Cosumnes river basin. Substantial changes to annual average temperature (>+2.5°C) and precipitation (>+38%) will characterize the EoC extreme water years compared to their historical counterparts. A shift in the dominant form of precipitation, mostly in the form of rain, is projected to fall earlier. These changes reduce snowpack by more than 90%, increase peak surface water and groundwater storages up to 75% and 23%, respectively, and drive the timing of peak storage to occur earlier in the year. Because EoC temperatures and soil moisture are high, both potential and actual evapotranspiration (*ET*) increase. The latter, along with the lack of snowmelt in the warm EoC, cause surface water and groundwater storages to significantly decrease in summer, with groundwater showing the highest rates of decrease. These changes result in more ephemeral EoC streams with more focused flow and increased storage in the mainstem of the river network during the summer.

Keywords: future climate extremes, integrated hydrologic model, global climate model, end of century hydrology, watershed hydrology, water management

Introduction

California, the fifth*largest economy in the world, hosts one of the largest agricultural regions in the United States and is home to over 39 million people. Because of its geographic location, Mediterranean climate, geology, and landscape, the state of California is sensitive to climate change (Hayhoe et al. 2004). Understanding how water resources will evolve under a changing climate is crucial for sustaining the state's economy and agricultural productivity. The region is especially susceptible to climate change given its reliance on the Sierra Nevada Mountain snowpack as a source of water supply (e.g., Dettinger & Anderson, 2015). Studies show that temperatures may warm by as much as 4.5°C by the End of Century (hereafter, EoC) (Cayan et al., 2008), that snowpack is expected to decrease as most precipitation will fall as rain instead of snow (Siirila-Woodburn, et al., 2021), and that rain on snow events will exacerbate melt (Cayan et al., 2008; Gleick, 1987; Maurer, 2007; Mote et al., 2005; Musselman, Clark, et al., 2017; Musselman, Molotch, et al., 2017; Rhoades, Ullrich, & Zarzycki, 2018a). Given that precipitation falls predominantly in winter months and the summers are hot and dry, the snow accumulated during the winter provides important water storage for the dry season and is crucial to meet urban demand, sustain ecosystem function, and maintain agricultural productivity (Bales et al., 2006; Dierauer et al., 2018). As such, any significant reduction in the snowpack has the potential to drastically affect the hydrology of the state (Barnett et al., 2005; Harpold & Molotch, 2015; Milly et al., 2005; Rhoades et al., 2018 a,b).

Over the past several decades, researchers have worked to understand how changes in Sierra Nevada snowpack will affect important hydrologic fluxes such as evapotranspiration (Tague & Peng, 2013) and streamflow (Berghuijs et al., 2014; Gleick, 1987; He et al., 2019; Maurer, 2007; Safeeq et al., 2014; Son & Tague, 2019; Vicuna & Dracup, 2007; Vicuna et al., 2007). For

example, analyses of recent historical trends show that reductions in snowpack result in increases in winter streamflow and decreases in the summer streamflow (e.g. Safeeq et al., 2012). However, the sensitivity of a given area to these climatic changes depends on many factors including geology and therefore drainage efficiency, topography, and land cover (Alo & Wang, 2008; Christensen et al., 2008; Cristea et al., 2014; Ficklin et al., 2013; Mayer & Naman, 2011; Safeeq et al., 2015; Son & Tague, 2019; Tang et al., 2019).

Climate change in California is also expected to lead to unprecedented extreme conditions, which include both severe drought and intense deluge (Swain et al., 2018). In recent years, these changes have already been observed in the forms of multi-year droughts (Cook et al., 2004; Griffin & Anchukaitis, 2014; Shukla et al., 2015) and high-intensity precipitation events mainly caused by atmospheric rivers (Dettinger et al., 2004; Dettinger, 2011; Dettinger, 2013; Ralph & Dettinger, 2011; Ralph et al., 2006). Periods without regular precipitation will require water management strategies to adapt to ensure demands are met. Similarly, risk management plans and/or infrastructure for floods, landslides, and other water surplus associated hazards (such as dam failure) may also require reconsideration. This will be especially true if periods of precipitation, including those associated with atmospheric rivers, become more extreme, variable, and occur over a shorter window of time (Swain et al., 2018; Gershunov et al., 2019; Huang et al., 2020; Rhoades et al., 2020b; Rhoades et al., 2021). Changes in water availability due to climate "whiplash" will also have important ramifications for water resource management (Wang et al., 2017; Swain et al., 2018) and significantly increase annual flood damages based on the level of global warming that occurs (Rhoades et al., 2021). For example, in just the last two decades, California has experienced the most severe drought in the last 1200 years (Griffin & Anchukaitis, 2014) followed by the wettest year on record (Di Liberto, 2017; SCRIPPS, 2017). These changes

82 in meteorological patterns may become the “new normal”, raising several outstanding questions
83 related to how these changes in climate will impact the integrated hydrologic cycle, and
84 subsequently water resource availability for humans and ecosystems.

85 To project how changes in climate will impact watershed behavior, high-resolution,
86 physics-based models are one of the most promising ways to simulate system dynamics accurately,
87 particularly those that are non-linear, and constitute a better way to analyze a no-analog future than
88 the models used in the previous works. Previous studies analyzed future hydrologic conditions in
89 California but relied on models that do not 1) account for the interactions, feedbacks, and
90 movements of water from the lower atmosphere to the subsurface; 2) represent groundwater
91 dynamics and lateral flow; 3) incorporate physics-based high-resolution climate models and/or 4)
92 hydrologic models (e.g., Berghuijs et al., (2014); Gleick, (1987); He et al., (2019); Maurer, (2007);
93 Safeeq et al., (2014); Son & Tague, (2019); Vicuna & Dracup, (2007); Vicuna et al., (2007)).
94 Considerations of coupled interactions that explicitly account for groundwater connections are
95 important (Condon et al., 2020, 2013; Maxwell and Condon, 2016), especially given groundwater
96 is the largest reservoir in the terrestrial hydrologic budget and integral to water resource
97 availability. Also, previous studies have focused on the mid-century period (e.g. Maurer & Duffy,
98 2005; Son & Tague, 2019), which may indicate a more muted signal in hydrologic impacts than at
99 EoC. Understanding these impacts is essential because long-term climate projections show that
100 extremes will be more frequent and significant by the EoC (Cayan et al., 2008).

101 In this work, we assess the impacts of EoC extremely dry and intensely wet conditions on
102 the hydrodynamics of a Californian watershed that contains one of the last naturally flowing rivers
103 in the state. This allows us to investigate the impacts of climate change without the complexity of
104 active water management, and thus to set the context for water management decisions. We

specifically investigate how the water and energy balance respond to climate extremes under climate change, and how those changes propagate to alter the spatiotemporal distribution of water in different hydrologic compartments of the watershed. We focus our investigation on the changes in groundwater and surface water storages. The balance of these two natural reservoirs, and their relationship in response to changes in snowpack reservoir changes, is important for water management decision making. We aim to 1) strengthen our physics-based understanding of the main hydrologic processes controlling changes in water storages under a changing climate, 2) quantify the magnitude and timing of these shifts in storage, and 3) identify the areas that are most vulnerable to change.

To do so, we utilize a novel combination of cutting-edge climate and hydrologic model simulations. We use an integrated hydrologic model (ParFlow-CLM; Maxwell & Miller, 2005), which solves the water-energy balance across the Earth's critical zone. When projecting hydrologic flows, ParFlow-CLM's explicit inclusion of three-dimensional groundwater flow is important given its demonstrated role in impacting land surface processes like evapotranspiration (Maxwell & Condon, 2016). We drive Parflow-CLM with climate forcing from a physics-based, variable-resolution enabled global climate model (the Variable Resolution enabled Community Earth System Model, VR-CESM; Zarzycki et al., 2014) that dynamically couples multi-scale interactions within the atmosphere-ocean-land system. This novel pairing of models allows for several key considerations not present in other methods. Our approach represents both dynamical and thermodynamic atmospheric response to climate change across scales, different from "pseudo-global warming" and "statistical delta" approaches used in many hydrologic modeling studies (e.g., Foster et al., 2020; Rasmussen et al., 2011). While these approaches are useful to isolate the impact of a given perturbation and/or variable, expected changes in climate will involve the co-

evolution of many processes, and may therefore not account for compensating factors. The interaction between dynamical and thermodynamic responses has important, and sometimes, offsetting effects on features such as atmospheric rivers. For example, Payne et al. (2020) show that the thermodynamic response to climate change enhances atmospheric river characteristics (e.g., Clausius-Clapeyron relationship), whereas the dynamical response diminishes atmospheric river characteristics (e.g., changes in the jet stream and storm track landfall location). Therefore, VR-CESM may simulate a more inclusive hydroclimatic response to climate change in the western United States at a resolution that is at the cutting-edge of today's global climate modeling capabilities for decadal-to-centennial length simulations (Haarsma et al., 2016).

We perform these couplings on spatial and temporal scales relevant for atmosphere-to-land, and land-to-subsurface interactions, an important consideration, given the recent work showing the importance of meteorological forcing resolution in representing the hydrologic cycle (Kampenhout et al., 2019; Maina et al., 2020b; Rhoades et al., 2016; Rhoades, Ullrich, Zarzycki, et al., 2018c; Wu et al., 2017). Climate conditions for EoC (2070-2100) and a 30-year historical period (1985-2015) are simulated to identify the median, wettest, and driest water year (WY) in each. We then simulate the subsequent watershed hydrology of each year using ParFlow-CLM forced with those meteorological conditions.

1. The Cosumnes watershed

The Cosumnes River is one of the last rivers in the western United States without a major dam, offering a rare opportunity to isolate the impacts of a changing climate on the hydrodynamics without reservoir management consideration (Maina et al., 2020a; Maina and Siirila-Woodburn, 2020). The watershed spans the Central Valley-Sierra Nevada interface and therefore represents

151 important aspects of the large-scale hydrology patterns of the state, namely the assessment of
152 interactions between changes in precipitation, snowpack, streamflow, and groundwater across
153 elevation and geologic gradients. Located in Northern California, USA, the Cosumnes watershed
154 is approximately 7,000 km^2 in size (Figure 1) and is between the American and the Mokelumne
155 rivers. Its geology ranges from low-permeability rocks typical of the Sierra Nevada landscape
156 (volcanic and plutonic) to the porous and permeable alluvial depositions of the Central Valley
157 aquifers. These are separated by very low-permeability marine sediments. The watershed
158 topography includes a range of landscapes typical of the region (e.g. varying from flat agricultural
159 land, rolling foothills, and steep mountainous hillsides), and elevation varies from approximately
160 2500 m in the upper watershed to sea level in the Central Valley (Figure 1). The Sierra Nevada
161 mountains are characterized by evergreen forest while the Central Valley hosts an intensive
162 agricultural region including crops such as alfalfa, vineyards, as well as pastureland. Like other
163 Californian watersheds, the climate in the Cosumnes is Mediterranean consisting of wet and cold
164 winters (with a watershed average temperature equal to 0°C) and hot and dry summers (with
165 watershed average temperature reaching 25°C) (Cosgrove et al., 2003).

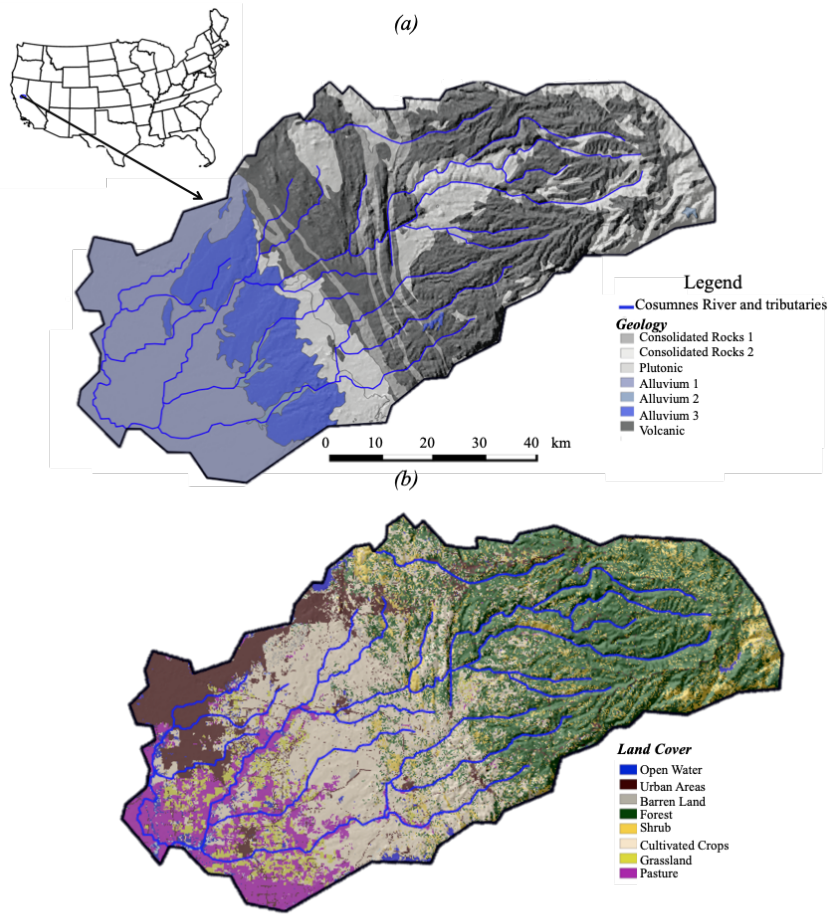

166

167 Figure 1: The Cosumnes Watershed (a) location and geology (Jennings et al., 1977), the alluvium
168 in blue corresponds to the Central Valley aquifers whereas the consolidated rocks in gray
169 correspond to the Sierra Nevada and cross-cutting marine sediments, and (b) land cover (Homer
170 et al., 2015).

171

172 **2. Experimental Design**

173 **2.1. Variable Resolution Community Earth System Model (VR-CESM)**

174 Historical and EoC meteorological forcings are obtained from a simulation using the VR-
175 CESM at a regionally refined resolution of 28 km over the Northern Pacific Ocean through the
176 western United States, including the Cosumnes watershed and a global resolution of 111 km

(Figure 2). CESM has been jointly developed by NCAR (National Center for Atmospheric Research) and the DOE (U.S. Department of Energy) and simulates a continuum of Earth system processes including the atmosphere, land surface, land ice, ocean, ocean waves, and sea ice and the interactions between them (Collins et al., 2006; Gent et al., 2011; Hurrell et al., 2013). VR-CESM is a novel tool to perform dynamical downscaling as it allows for the interactions between the major components of the global climate system (e.g., atmosphere, cryosphere, land surface, and ocean) while allowing for regional-scale phenomena to emerge where regional refinement is applied, all within a single model (Huang et al., 2016; Rhoades et al., 2016; Rhoades, Ullrich, & Zarzycki, 2018b; Rhoades, Ullrich, Zarzycki, et al., 2018c).

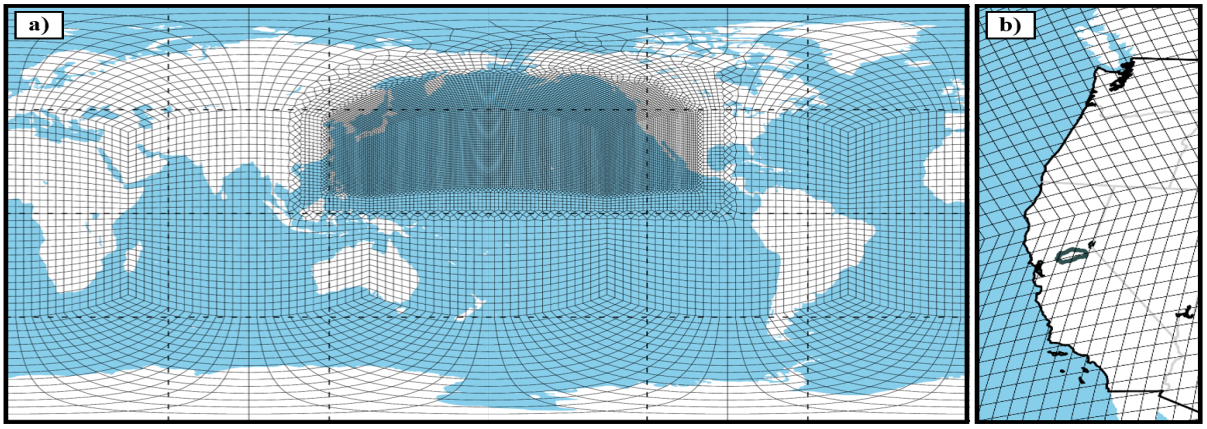

Figure 2: Variable Resolution Community Earth System Model (VR CESM) grid for (a) globe and (b) coastal western US with the Cosumnes watershed overlaid in dark gray.

The atmospheric model used for these simulations is the Community Atmosphere Model (CAM) version 5.4 with the spectral element dynamical core, with an atmospheric dynamics time step of 75 seconds, an atmospheric physics time step of 450 seconds, a prognostic treatment of rainfall and snowfall in the microphysics scheme (Gettelman and Morrison, 2015) and run under Atmosphere Model Intercomparison Project (AMIP) protocols (Gates, 1992). Under the AMIP protocols, the atmosphere and land-surface components of the Earth system model are coupled

and periodically bounded by monthly observed sea-surface temperatures and sea-ice extents. Although this configuration does not exactly recreate historical water years and events, it is expected to reasonably simulate the distribution of water year types. Also, it should be noted that the model only projects future conditions, within the envelope of plausible future conditions of the RCP8.5 scenario and its assumptions of greenhouse gas emissions, sea-surface temperatures, and sea ice extents and would not be expected to exactly forecast individual water years. Simulations with VR-CESM are performed for 30-year periods based on the climates from a historical period (1985-2015) and an EoC period (2070-2100). EoC simulations, analogous to Rhoades, Ullrich, & Zarzycki, 2018, are bounded by estimates of future changes in ocean conditions derived from a fully-coupled bias-corrected CESM simulation (assuming historical ocean simulation biases will be similar in the future simulation) and forced by greenhouse gases and aerosol concentrations assumed in the RCP8.5 emissions scenario. Historical VR-CESM outputs have been compared with reanalyses and future VR-CESM outputs have been analyzed for shifts in hydrometeorological extremes in further detail in Rhoades et al., 2020 a,b. To couple the outputs with ParFlow-CLM, we regrid the unstructured 28km VR-CESM data over the Cosumnes watershed using bilinear interpolation in the Earth System Modeling Framework (Jones, 1999) to a final resolution of approximately 11 km (i.e., 57 grids over the Cosumnes watershed). Notably, each of the spectral elements in the VR-CESM grid, shown in Figure 1, has a 4x4 set of Gauss–Lobatto–Legendre (GLL) quadrature nodes where equations of the atmospheric model are solved (Herrington et al., 2019). Therefore, the actual resolution at which the atmospheric dynamics and physics are solved in VR-CESM are at higher-resolution (~28km) than is shown in Figure 1, making these some of the highest resolution global Earth system model simulations over California to date (Haarsma et al., 2016).

To identify if VR-CESM is fit for purpose to simulate historical dry, median, and wet WYs, and inform potential biases in future projections (over California and, more specifically, the Cosumnes watershed), we first conduct a model comparison to a widely used observational product, the Parameter-elevation Relationships on Independent Slopes Model (PRISM; Daly et al., 2008) at 4 km resolution analogous to Rhoades et al., (2020a). However, in this study, we focus our assessment of VR-CESM fidelity over California and the Cosumnes watershed. PRISM provides daily precipitation, mean dewpoint temperature and maximum and minimum surface temperature, and vapor pressure. PRISM precipitation and temperature data spanning 1981-2019 are compared with the VR-CESM 1985-2015 simulations. We note that a mismatch in the time period (1981-2019 versus 1985-2015) is deliberate. As stated previously, VR-CESM is simulated under AMIP-protocols (bounded by monthly observed sea-surface temperatures and sea-ice extents), and therefore we do not expect VR-CESM to exactly recreate past historical WYs. However, we do expect that our 30-year simulation can reasonably recreate the range of WY types over California and the Cosumnes, which is why we utilize the broader range of PRISM WYs that are available. For this comparison, we regrid the unstructured VR-CESM data to 4km resolution (the native resolution of PRISM) using the Earth System Modeling Framework (ESMF) Offline Re-gridding Weight Generator in the NCAR Command Language (NCL, 2021).

The comparison (discussed in appendix A) indicates that VR-CESM reasonably reproduces the historical WY conditions (i.e., interannual range of PRISM precipitation largely overlaps with the range of model bias simulated by VR-CESM). VR-CESM generally simulates a wetter historical period over the Cosumnes (range of bias of 1330 mm) relative to PRISM (range of interannual variability of 1320 mm). Basin-average minimum (421 mm) and maximum (1740 mm) WY accumulated precipitation are slightly larger than those of PRISM. Of relevance to this study,

PRISM has shown notable uncertainties in the Sierra Nevada. Lundquist et al., 2015 showed that an underrepresentation of the most extreme storm total precipitation in the Sierra Nevada can result in an upper-bound uncertainty of 20% in WY accumulated precipitation in PRISM. Therefore, the wettest WY simulated by VR-CESM is well within the 20% uncertainty range of PRISM's wettest WY (1580 ± 316 mm). Further, differences in basin-average WY accumulated precipitation between VR-CESM and PRISM are non-significant using a t-test and assuming a p-value < 0.05. As discussed in further detail below, we posit that atmospheric river-related precipitation is likely the driver of the wet bias mismatch with PRISM. However, we also note that the uncertainty bounds of the PRISM product WY precipitation totals in the Sierra Nevada are estimated to be upwards of ~20% too dry (e.g., Lundquist et al., 2015), particularly for extreme precipitation events such as atmospheric rivers and in mountainous terrain.

2.2. Integrated Hydrologic Model: ParFlow-CLM

The integrated hydrologic model ParFlow-CLM (Kollet & Maxwell, 2006; Maxwell, 2013; Maxwell & Miller, 2005) solves the transfer and interactions of water and energy from the subsurface to the lower atmosphere including groundwater dynamics, streamflow, infiltration, recharge, evapotranspiration, and snow dynamics. The model describes 3D groundwater flow in variably saturated media with the Richards equation (equation 1, Richards, 1931) and 2D overland flow with the kinematic wave equation (equation 2).

$$S_S S_W(\psi_P)\frac{\partial \psi_P}{\partial t} + \phi\frac{\partial S_W(\psi_P)}{\partial t} = \nabla.\left[K(x)k_r(\psi_P)\nabla(\psi_P - z)\right] + q_s \quad (1)$$

Where is S_S the specific storage (L^{-1}), $S_W(\psi_P)$ is the degree of saturation (-) associated with the subsurface pressure head ψ_P (L), t is the time (T), ϕ is the porosity (-), k_r is the relative

permeability (-), z is the depth, q_s is the source/sink term (T^{-1}) and $K(x)$ is the saturated hydraulic conductivity ($L\ T^{-1}$).

ParFlow solves the mixed form of the Richards equation which has the advantage of conserving the mass (Celia et al., 1990).

The kinematic wave equation is used to describe surface flow in two dimensions is defined as:

$$-k(x)k_r(\psi_0)\nabla(\psi_0 - z) = \frac{\partial\|\psi_0,0\|}{\partial t} - \nabla.\vec{v}\|\psi_0,0\| - q_r(x) \quad (2)$$

Where ψ_0 is the ponding depth, $\|\psi_0,0\|$ indicates the greater term between ψ_0 and 0, $\vec{v}$ is the depth averaged velocity vector of surface runoff ($L\ T^{-1}$), q_r is a source/sink term representing rainfall and evaporative fluxes ($L\ T^{-1}$).

Surface water velocity at the surface in x and y directions, (v_x) and (v_y) respectively, is computed using the following set of equations:

$$v_x = \frac{\sqrt{S_{f,x}}}{m}\psi_0^{\frac{2}{3}} \text{ and } \quad v_y = \frac{\sqrt{S_{f,y}}}{m}\psi_0^{\frac{2}{3}} \quad (3)$$

Where $S_{f,x}$ and $S_{f,y}$ friction slopes along x and y respectively and m is the manning coefficient. ParFlow employs a cell-centered finite difference scheme along with an implicit backward Euler scheme and the Newton Krylow linearization method to solve these nonlinear equations. The computational grid follows the terrain to mimic the slope of the domain (Maxwell, 2013).

ParFlow has many advantages in comparisons to other hydrologic models. Compared to other hydrologic models (MODFLOW (Harbaugh, 2005), FELFOW (Trefry and Muffels, 2007), SWAT (Soil and Water Assessment Tool) (Neitsch et al., 2000), SAC-MA (Sacramento Soil Moisture Accounting Model)), ParFlow has the advantages of accounting for land surface processes such as snow dynamics and evapotranspiration and their interactions with the subsurface which are crucial for studying the hydrology of California. ParFlow also solved the subsurface

flow by accounting for variably saturated conditions, an important feature for calculating groundwater recharge and the connection between the groundwater and the land surface processes, which is not the case for the aforementioned models. While some hydrologic models have a better representation of the land surface processes (Noah-MP (Niu et al., 2011), VIC (Variable Infiltration Capacity Model Macroscale Hydrologic Model) (Liang et al., 1994)), these models do not have a detailed representation of the subsurface flows. Because the surface flow is important in the region and it establishes the connection between the headwaters and the valleys, its good representation is essential for projecting changes in hydrology. Compared to other integrated hydrologic models (CATHY (Catchment Hydrology) (Bixio et al., 2002), MIKE-SHE (Abbott et al., 1986)), ParFlow has the advantages of solving a two-dimensional kinematic flow equation that is fully coupled to the Richards equation.

ParFlow is coupled to the Community Land Model (CLM) to solve the surface energy and water balance, which enables interactions between the land surface and the lower atmosphere and the calculation of key land surface processes governing the system hydrodynamics such as evapotranspiration, infiltration, and snow dynamics. CLM models the thermal processes by closing the energy balance at the land surface given by:

$$R_n(\theta) = LE(\theta) + H(\theta) + G(\theta) \quad (4)$$

Where $\theta = \phi S_w$ is the soil moisture, R_n is the net radiation at the land surface (E/LT) a balance between the shortwave (also called solar) and longwave radiation, LE is the latent heat flux (E/LT) which captures the energy required to change the phase of water to or from vapor, H is the sensible heat flux (E/LT) and G is the ground heat flux (E/LT).

More information about the coupling between ParFlow and CLM can be found in Maxwell & Miller, (2005). CLM uses the following outputs of the VR-CESM model at 3-hourly resolution

310 to solve the energy balance at the land surface: precipitation, air temperature, specific humidity,
311 atmospheric pressure, north/south and east/west wind speed, and shortwave and longwave wave
312 radiation.

313 We constructed a high-resolution model of the Cosumnes watershed with a horizontal
314 discretization of 200 m and vertical discretization that varies from 10 cm at the land surface to 30
315 m at the bottom of the domain. The model has 8 layers, the first 4 layers represent the soil layers
316 and the other four the deeper subsurface. The total thickness of the domain is 80 m to ensure
317 appropriate representation of water table dynamics. Observed water table depths (as measured at
318 several wells located in the Central Valley portion of the domain) vary between approximately 50
319 m and the land surface through a multi-year time period (Maina et al., 2020a). Therefore, to be
320 conservative for imposing the lower boundary layer, anything below 80 m is expected to remain
321 fully saturated. The resulting model comprises approximately 1.4 million active cells and was
322 solved using 320 cores in a high-performance computing environment. The Cosumnes watershed
323 is bounded by the American and Mokelumne rivers. We, therefore, impose weekly varying values
324 of Dirichlet boundary conditions along these borders to reflect the observed changes of river
325 stages. The eastern part of the watershed corresponding to the upper limit in the Sierra Nevada is
326 modeled as a no-flow (i.e., Neumann) boundary condition. Hydrodynamic parameters required to
327 solve the surface and subsurface flows (e.g., hydraulic conductivity, specific storage, porosity, and
328 van Genuchten parameters) are derived from a regional geological map (Geologic Map of
329 California, 2015; Jennings et al., 1977) and a literature review of previous studies (Faunt et al.,
330 2010; Faunt and Geological Survey (U.S.), 2009; Gilbert and Maxwell, 2017; Welch and Allen,
331 2014). We use the 2011 National Land Cover Database (NLCD) map (Homer et al., 2015) to
332 define land use and land cover required by CLM. We further delineate specific croplands (notably

alfalfa, vineyards, and pasture) in the Central Valley by using the agricultural maps provided by the National Agricultural Statistics Service (NASS) of the US Department of Agriculture's (USDA) Cropland Data Layer (CDL) (Boryan et al., 2011). Vegetation parameters are defined by the International Geosphere-Biosphere Programme (IGBP) database (IGBP, 2018). A complete description of the model parameterization can be found in appendix B and more details in Maina et al. (2020a). The model has been extensively calibrated and validated using various datasets, including remotely sensed data and ground measurements, which are however very sparse in the area. Model validation which consists in comparing both surface and subsurface hydrodynamics (groundwater and river stages) and land surface processes was performed over a period of three years that includes extremely dry and wet water years (Appendix C). We specifically compared simulated and measured river stages at three stations located in the Sierra Nevada headwater, foothill, and the Central Valley. The annual averages absolute differences between measurements and simulations were between 0.4 and 0.8 m. We selected four wells in the Cosumnes watershed based on their availability of data to compare measured and simulated groundwater levels. These wells are sparsely distributed in the Central Valley. The absolute differences between observed and simulated groundwater levels vary between 0.47 to 3.73 m. The highest absolute differences were attributed to the lack of best estimations of groundwater pumping rates in the region. Nonetheless, the reasonable agreement between observations and simulated variables over a period that includes both extremely dry and intensely wet conditions has allowed us to conclude that the model can capture these extreme dynamics. We rely on remote sensing data to assess the ability of our model to simulate key land surface processes (evapotranspiration *ET*, soil moisture, and snow water equivalent *SWE*). We compared the simulated *SWE* to SNODAS (The National Weather Service's Snow Data Assimilation, National Operational Hydrologic

356 Remote Sensing Center, 2004) and a *SWE* reanalysis by Bair et al., (2016). Our comparisons
357 indicated that the absolute differences between our *SWE* values and these data were equal to 3 mm
358 on average. Moreover, the simulated key parameters controlling the snow dynamics such as peak
359 snow and timing of snow ablation were also in agreement with remotely sensed data for both dry
360 and wet years (Appendix C). Absolute differences between the simulated *ET* and the remotely
361 sensed *ET* from METRIC (Mapping Evapotranspiration at High Resolution with Internalized
362 Calibration, Allen et al., 2007) were equal to 0.036 mm/s while the differences between the
363 simulated soil moisture and the SMAP (Soil Moisture Active Passive, SMAP, 2015) soil moisture
364 were 0.2. More details about model calibration and validation can be found in Appendix C and
365 previous publications (Maina et al., 2020a, Maina et al., 2020b; Maina and Siirila-Woodburn,
366 2020c). The model has also been successfully used in recent investigations of post-wildfire and
367 climate extremes hydrologic conditions and to assess the role of meteorological forcing scale on
368 simulated watershed dynamics (Maina et al., 2020a, b; Maina and Siirila-Woodburn, 2020c).
369 Initial conditions for pressure-head were obtained by a spin-up procedure using the forcing of the
370 historical median WY. We recursively simulated the historical median WY forcing until the
371 differences of storage at the end of the WY were less than 1%, indicating convergence. This
372 pressure head field is then used as the initial condition for each of the five WYs of interest (i.e.,
373 the EoC wet, EoC dry, historic wet, historic dry, EoC median). Though we acknowledge land
374 cover alterations are expected to occur by the EoC (either naturally or anthropogenically), in this
375 work we assume that the vegetation remains constant for both historical and EoC simulations for
376 simplicity. Although outside of the scope of this work, future studies will investigate the impacts
377 of an evolved land use/land cover, vegetation physiology, and resilience strategies to manage water
378 resources. Further, while the Central Valley of California hosts intensive agriculture that is reliant

on groundwater pumping for irrigation, we didn't incorporate pumping and irrigation in our model configuration. We did this with the assumption that groundwater pumping rates may substantially change in the future due to new demands, policies, regulations, and changes in land cover and land use and aim to provide an estimate of the natural hydrologic system response to climate change.

2.3. Analysis of EoC hydrodynamics

To investigate how the EoC climate extremes affect water storages, we investigate five hydrologic variables: *SWE*, *ET*, Pressure-head (ψ) distributions, and surface and subsurface water storage. Total groundwater (GW) storage is given by:

$$Storage_{GW} = \sum_{i=1}^{n_{GW}} \Delta x_i \times \Delta y_i \times \Delta z_i \times \psi_i \times \left(\frac{S_{si}}{\phi_i}\right) \quad (5)$$

where n_{GW} is the total number of subsurface saturated cells (-), Δx_i and Δy_i are cell discretizations along the x and y directions (L), Δz_i is the discretization along the vertical direction the cell (L), S_{s_i} is the specific storage associated with cell i, ψ_i the pressure-head, and ϕ_i is the porosity.

Total surface water (SW) storage which accounts for any water located at the land surface (i.e., any cell of the model with a pressure-head greater than 0) and includes river water or overland flow is calculated via:

$$Storage_{SW} = \sum_{i=1}^{n_{SW}} \Delta x_i \times \Delta y_i \times \psi_i \quad (6)$$

where n_{SW} is the total number of cells with surface water i.e., with surface ψ greater than 0 (-), and i indicates the cell.

We compare each EoC WY simulation to its corresponding historical WY counterpart and both the historical and EoC medians. This allows us to assess how EoC extremes change relative to what is currently considered an extreme condition as well as to "normal" in the relevant time. Comparisons are shown as a percent change (*PC*) calculated using:

$$PC_{i,t} = \frac{X_{projection_{i,t}} - X_{baseline_{i,t}}}{X_{baseline_{i,t}}} \times 100 \quad (3)$$

where X is the model output (ET, SWE, or ψ) at a given point in space (i) at a time (t), *baseline* is the selected simulation (historical median, EoC median, or historical extreme), and *projection* represents the simulation obtained with the EoC extreme WYs (dry or wet).

3. Results

In this section, we present a subset of the outputs from VR-CESM (precipitation and temperature) to identify the extreme (dry and wet) and median WYs of interest. Changes in fluxes and storages over the course of each WY, as well as the spatial variability of these changes in two important periods of the WY (peak flow and baseflow) are also shown.

3.1. Selection of the median, dry, and wet WYs

From the historical and EoC 30-year VR-CESM simulations we select the median, wettest, and driest WYs for comparison (see Figure 3a). Overall, the future WYs are ~30% wetter than the historical WYs (p-value ~0.006 for two-tailed t-test of equal average annual precipitation) in addition to being ~4.6ºC warmer. Precipitation and temperature variances are mostly similar in the historical and EoC simulations, though EoC minimum temperature may be more variable (p-value ~0.059 for two-tailed f-test of equal variance in minimum temperature). On average the timing for the start, length, and end of precipitation is similar, though EoC precipitation may be less variable in its start time (p-value ~0.053 for f-test of equal variance in days to reach 5th percentile of annual precipitation). In the climate model, there are no clear trends between the precipitation timing metrics and total amount of precipitation.

The EoC median WY is much wetter than its historical counterpart, with about ~250 mm more precipitation that begins approximately 1 week earlier and ends approximately 2 weeks earlier in the year. The EoC wettest WY is much wetter than the historical wettest WY and is characterized by 42% more precipitation. This is consistent with Allan et al. (2020), who suggest a wetter future. The EoC wettest WY is 3.8ºC warmer than the historical wettest WY and 4.6ºC warmer than the historical median WY, as the historical median WY is one of the coolest years in the series. Precipitation occurs earlier in the EoC wet WY compared to the historical wet or median WYs, with the 5th percentile of precipitation reached 12 days earlier in the EoC wettest WY than either the wettest or median historical WYs. The duration of the EoC wettest WY precipitation season (146 days) is between the historical wettest WY (133 days) and the historical median WY (155 days).

The EoC dry WY is also much wetter than its historic counterpart; in fact, the EoC dry WY is wetter than the seven driest historical WYs of the 30-year historical ensemble. Simulation of 30 random draws from two identical normal distributions, repeated 100,000 times, finds that the lowest value in one is higher than the seven lowest values in the other only ~1.1% of the time (p-value ~0.011). This statistical test reveals that this VR-CESM simulation suggests that future dry years will be somewhat wetter than historical dry years. The EoC dry WY is only ~2.5ºC warmer than the historical dry WY. The divergence in temperature is smaller for the comparison of EoC and historical WYs of the dry extremes as opposed to the wet extremes because the historical dry WY is the second-warmest WY in the historical simulations, while the EoC dry WY is the third coolest in the EoC simulations. Precipitation in the EoC dry WY starts particularly early, with the 5th percentile of annual precipitation reached by mid-October. This is much earlier than either the dry or median historical WYs, which don't reach that percentile of precipitation until mid-to-late

November. The historical dry WY also has a particularly short precipitation duration of only 97 days, while the EoC dry WY has a 163-day precipitation duration, more similar to the median historical WY duration of 155 days.

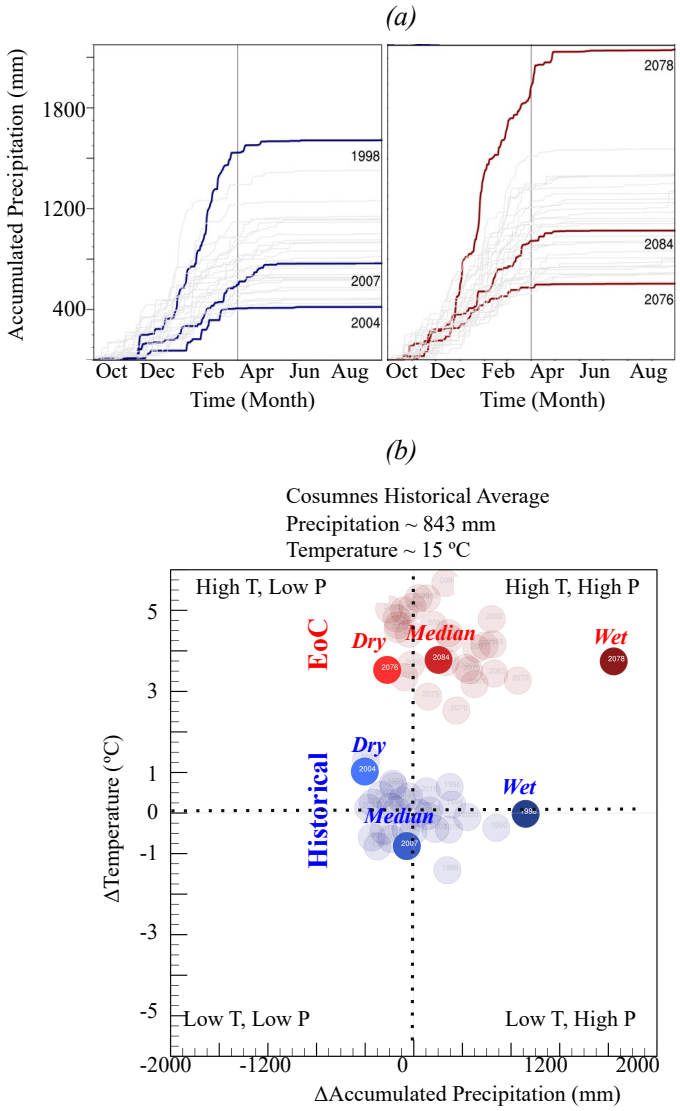

Figure 3: (a) VR-CESM accumulated total precipitation for the historical and End of Century (EoC) simulations, and (b) quadrants for differences between each individual water year (WY) and the historical average temperature and accumulated precipitation in the Cosumnes watershed. The historical and EoC dry, median and wet WYs are indicated in blue and red, respectively.

Figure 4 shows the spatial distribution of accumulated precipitation anomalies across California. These anomalies are computed for each of the six identified WYs relative to the climatological average (the 30-year historical mean). These spatial plots provide context for the changes modeled in the Cosumnes watershed relative to broader precipitation changes California-wide. As in the Cosumnes, California-wide EoC dry, median, and wet WYs are all characterized by higher precipitation totals than their historical counterparts. Importantly, the EoC wet WY is a true outlier not only in the Cosumnes but across California too. California lies at an important large-scale circulation transition, namely semi-permanent high-pressure systems associated with the Hadley circulation. Therefore, how climate change alters the atmospheric dynamics over California, or more specifically how far northward storm-tracks may shift, remains uncertain and depends on climate model choice. This has led to papers that claim the future of California will be wet across a range of climate models (e.g., Neelin et al, 2013; Swain et al., 2013; Gershunov et al., 2019; Rhoades et al., 2020b; Persad et al., 2020) and, for select climate models, that it could be drier. Notably, these studies highlight an asymmetric response in the frequency of wet versus dry WYs (i.e., anomalously wet WYs increase in frequency much more in the future than anomalously dry WYs). Many of the aforementioned studies also highlight that in anomalously wet WYs extreme precipitation events (e.g., atmospheric rivers) will occur with greater intensity and frequency and largely drive changes in WY precipitation totals (which is shown in our VR-CESM simulations for California in more detail in Rhoades et al., 2020b). Given these complexities and others such as consideration for how dynamical and thermodynamical effects of climate change may interact with one another to offset or amplify extreme precipitation events (Payne et al., 2020), the hypothesis that global warming will result in a climate where the "wet gets wetter and dry gets drier" may be too simplistic of an assumption for California. Rhoades et al., (2020b) shows

quantitatively that the increases in precipitation observed in the VR-CESM outputs are due to a greater number of intense atmospheric river events that occur more regularly back-to-back, which was recently corroborated by Rhoades et al. (2021) using uniform-high-resolution CESM simulations at different warming scenarios, and that atmospheric river precipitation totals increase at a much larger rate (+53%/K) than non-AR precipitation totals (+1.4%/K), which agrees with findings made in other studies such as Gershunov et al. (2019).

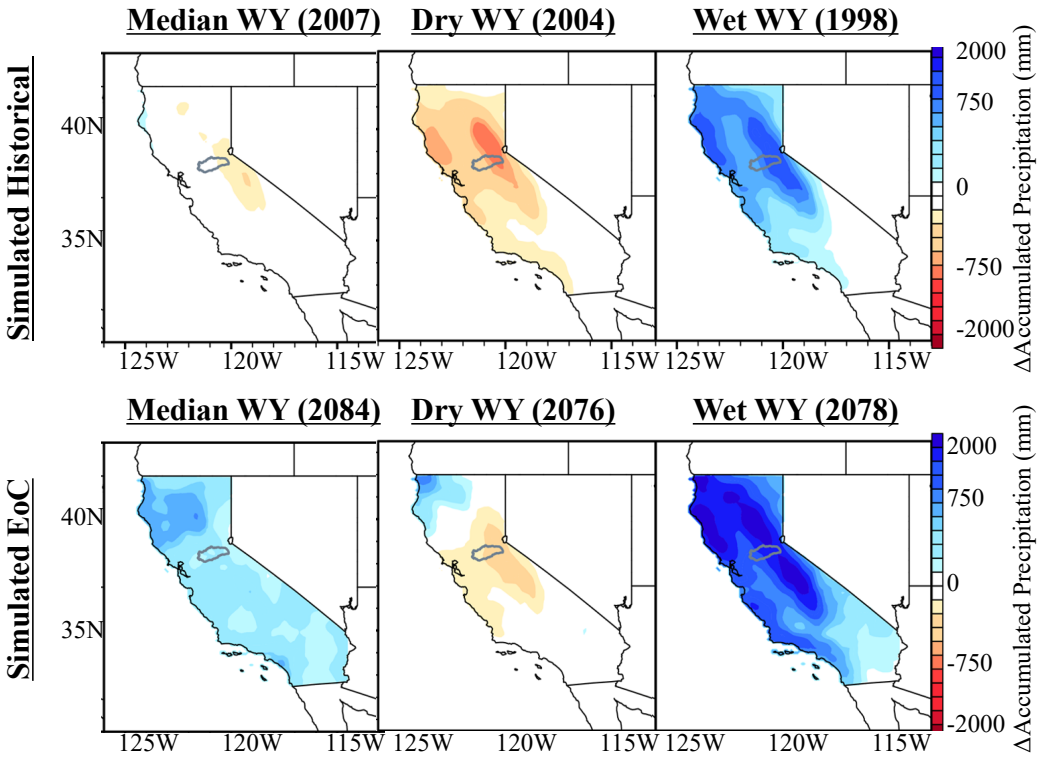

Figure 4: Precipitation spatial distributions of the dry, median, and wet water years (WY) for the 30-year historical and EoC simulations relative to the climatological average (derived from the 30-year historical mean)

3.2. Changes in annual watershed-integrated fluxes and storages

Figure 5 illustrates the annual changes in the integrated hydrologic budget of the Cosumnes watershed for the EoC WYs (i.e., median, dry, and wet) compared to the historical median WY.

The EoC median WY compared to the historical median WY has 38% more precipitation and the temperature is 4.4°C higher. Further, the precipitation phase also shifts with an increase in rainfall (54%) and a decrease in snowfall (-54%). This results in a significant decrease in *SWE* (-91%) which is consistent with many other studies that have shown that increased temperatures due to climate change will lead to low-to-no snow conditions (Berghuijs et al., 2014; Cayan et al., 2008; Mote et al., 2005; Rhoades et al., 2018 a,b; Son & Tague, 2019). The increase in temperature and precipitation results in an increase in *ET* (62%), consistent with the findings of other recent studies (e.g. McEvoy et al., 2020). Nevertheless, the larger amount of precipitation associated with the EoC is enough to offset higher *ET* demand and recharge groundwater and surface water, which experience an increase of 4% and 19% respectively. The EoC wet WY has similar changes as the EoC median WY when compared to the historical wet WY yet the magnitude of the increase in surface (21%), and groundwater (11%) storages are higher due to more precipitation and higher temperatures. The dry EoC WY is also characterized by higher precipitation (43%, the largest increase) than its historical counterpart, this results in large increases in total groundwater (8%) and surface water (38%) storages.

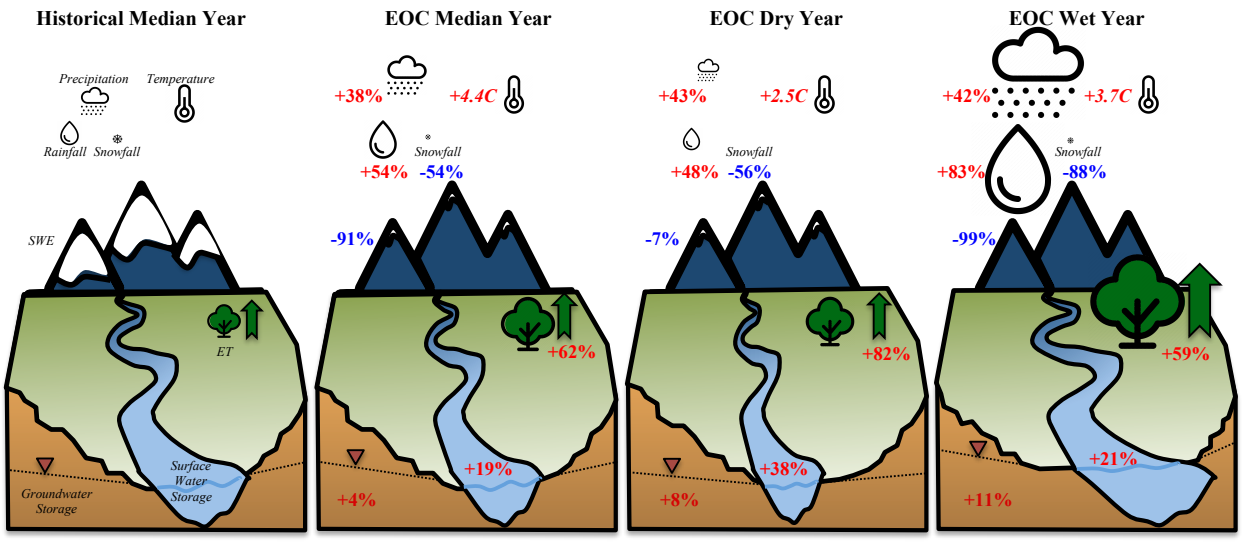

Figure 5: Annual percent changes in precipitation, rainfall, snowfall, temperature, *SWE*, *ET*, surface water, and groundwater storages in the EoC water years (WY) (i.e median, dry, and wet) at the watershed scale relative to their historical counterparts. Info-graphic size scaled to EoC conditions.

3.3. Temporal variation of watershed-integrated fluxes and storages

Understanding the annual changes at the watershed scale is important to broadly understand changes in the water budget in response to future climate extremes. However, a deeper understanding of the processes that drive these changes and the interactions from atmosphere-through-bedrock requires an analysis of their spatiotemporal variations as well. Figure 6 shows the temporal variations of each of the historical and EoC WY's integrated hydrologic budgets grouped by WY type (columns), with a top-down sequencing of hydrologic variables of interest in order from the atmosphere through subsurface (rows). This organization allows for the investigation of propagating impacts to be directly compared in time. In this section, we discuss historical vs EoC changes observed in each of the WY types (i.e., median, dry, and wet). Each WY shows unique hydrodynamic behaviors and changes compared to the historical conditions. The median WY sheds light on how changes in the precipitation phase and increases in temperature and precipitation in the EoC will impact the hydrodynamics. The dry WYs allow comparing EoC and historical low-to-no snow conditions whereas assessing the hydrodynamics of the EoC wet WY provides a better understanding of how intense EoC precipitation along with the warm EoC climate will shape the hydrology.

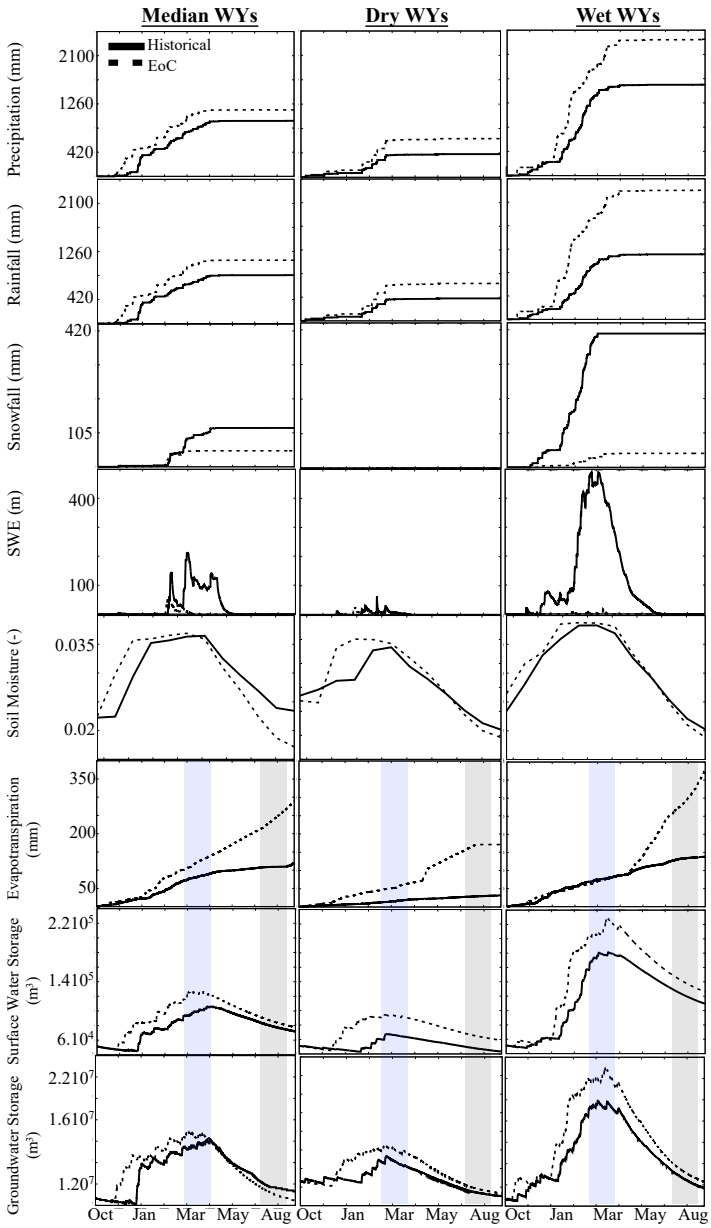

Figure 6: Temporal variations of the total cumulative precipitation, rainfall, and snowfall at the watershed scale, total *SWE* at the watershed scale, the average watershed values of soil moisture, the cumulative watershed *ET*, and the total surface water, and groundwater storages at the watershed scale associated with the six historical and EoC Water Years (WY). The blue area indicates the selected peak flow period while the gray area corresponds to the selected baseflow conditions for the spatial distribution analyses.

3.3.1. Median water years

As indicated in section 3.1, the EoC median WY has more precipitation than the historical median WY. The EoC precipitation comes mainly as rain due to the warmer temperatures of the EoC and includes virtually no snowfall from late winter to early spring. This precipitation phase-change combined with the earlier snowfall cessation date in the WY results in minimal and even non-existent *SWE* in the Cosumnes watershed for much of the WY, a significant change compared to historic conditions. EoC peak *SWE* occurs in February in contrast to the historical peak *SWE*, which occurs in April. Due to the watershed's relatively low elevation, snow accumulates only in the upper part of the Cosumnes watershed (~10% of the total watershed area). Only areas located in the highest elevations (> 2000 m), such as the eastern limit of the watershed, show any *SWE* in the EoC simulations whereas in the historical WYs we observed *SWE* as low as 1000 m.

The decrease in snow and the increase in rain along with an earlier onset of seasonal precipitation directly impacts soil moisture, which sees an early increase with a slightly higher peak than historical. As more water is available earlier in the EoC, the *ET* demand from increased temperatures is met until substantially higher summer temperatures increase *ET* at a much faster rate than the historical WY. The high EoC *ET* and the lack of snowmelt cause the soil to rapidly dry from late-spring through late-summer.

Because of the marked increase in total precipitation and shift from snow to rain in the EoC simulations, surface water storage generally increases throughout the WY. This is consistent with previous studies (Gleick, 1987; He et al., 2019; Maurer, 2007; Safeeq et al., 2014; Son & Tague, 2019; Vicuna & Dracup, 2007; Vicuna et al., 2007). Surface water storage increases in early November in the EoC simulations while in the historical simulations this increase occurs in

January. Similar to the earlier peak *SWE* and soil moisture, the peak surface water storage in the EoC is also earlier (January through February) compared to the historical period (March through April). This late-season surface water storage remains larger because the accumulated precipitation is large enough to overcome the increased *ET* in a warmer climate. Similar to surface water storage, groundwater storage increases earlier and peaks at a larger amount than the historical WY. However, in contrast to the surface water storage, the groundwater storage during baseflow conditions is lower in the median EoC compared to the median historical year. This decrease in groundwater during baseflow conditions is due to the lack of snowmelt and higher EoC *ET*. In late spring and summer in the EoC, groundwater keeps depleting through *ET* and is not recharged by snowmelt through surface and subsurface flows from the Sierra Nevada as in the historical period. This may indicate that compared to surface water storages, groundwater storage may be more sensitive to EoC hydroclimatic changes (which are multi-fold, and in this case include an increase in precipitation, a transition from snow to rain, and higher *ET*). One way to quantitatively measure this sensitivity is to compare the seasonal change in water storage between peak and baseflow conditions. Historically, changes between peak and baseflow conditions (i.e., the amount of water lost between peak and base flow) resulted in moderate seasonal changes in groundwater storage (30%) and surface water storage (32%). The EoC simulations reveal larger seasonal variation for groundwater and surface water storage (40% and 37% decreases, respectively). Groundwater in the Cosumnes Watershed is mainly recharged in the headwaters and stored in the Central Valley. Therefore, these Central Valley aquifers experience earlier and larger increases in storage which lead to more water available to *ET* and therefore aquifer depletion. A deeper understanding of this phenomenon requires an analysis of the spatial patterns of these changes which is performed later on in this study.

583

584 **3.3.2. Dry water years**

585 All EoC WYs are characterized by higher precipitation in the form of rainfall compared to
586 their historical counterparts. The historical dry WY has ~43% less total precipitation than the EoC
587 dry WY. However, we note that for the EoC dry WY the decrease in snowfall is less drastic than
588 the median or wet EoC years. This is because the historically driest WY is significantly warmer
589 than the historical average WY, and therefore already has a smaller snowpack, 94% lower than the
590 historical median WY. The EoC dry WY *SWE* also accumulates two months earlier than the
591 historical *SWE*. Because the differences in *SWE* between the dry WYs are smaller than the
592 differences in *SWE* between the median WYs (7% versus 91%), we can deduce that the early and
593 larger rise in soil moisture in the EoC dry WY is mostly due to an earlier and larger amount of
594 rainfall. The higher soil moisture and EoC temperatures result in higher *ET* throughout the WY
595 compared to the historical WY. This *ET* results in lower soil moisture by the end of the summer,
596 similar to the median WY. In addition, surface water storage peaks earlier and at a larger amount
597 compared to the historical WY. The surface water storage in the EoC remains higher throughout
598 the WY compared to its historical counterpart despite this higher *ET* due to the low precipitation
599 associated with the historical dry WY. We further note that the difference in surface water storage
600 during baseflow conditions between the two dry WYs is higher than the difference between the
601 two median WYs. The groundwater recharge starts two months earlier in the EoC driest WY
602 compared to the historical driest WY due to the changes in timing and magnitude of precipitation.
603 However, it is interesting to note that groundwater storage during baseflow conditions in the EoC
604 WY is nearly equal to the historical WY (within 3%). Thus, although more water enters the EoC
605 dry WY system through greater precipitation, it eventually exits by the end of the WY and no

606 considerable net gains to groundwater are observed. This significant reduction in groundwater
607 storage from late winter to end-of-summer is a result of the much larger EoC *ET* and highlights
608 the dynamic nature of the EoC dry year watershed interactions. Also similar to the median WY,
609 dry WY seasonal decreases in EoC storage are more pronounced in the groundwater signal (36%)
610 than in the surface water signal (33%). We further note that the decreases in groundwater and
611 surface water storages are, as in the median WY, larger (+8%) than the historical decreases.
612
613 **3.3.3. Wet water years**
614 The EoC wet WY is significantly wetter than all other WYs. Yet, unlike the historical WY,
615 the precipitation largely comes as rain, as shown by the low-to-no snowfall and *SWE* totals (Figure
616 6). The difference in future versus contemporary wet WY *SWE* (99%) is larger than the differences
617 between the median and the dry WYs (91%). As in other WYs, soil moisture increases earlier
618 compared to the historical wet WY. A greater water availability enables the system to meet the
619 high EoC *ET* demand. Hence, *ET* in the EoC wettest year remains higher than the historical wettest
620 year *ET* throughout the WY. However, the increase in *ET*, combined with the lack of snowmelt
621 that can buffer and recharge soil moisture in spring, leads to less soil moisture at the end of the
622 WY compared with the historical WY. Further, surface water storage increases earlier and at a
623 much faster rate in the EoC WY compared to the historical WY. This is mirrored in the
624 groundwater storages. As in the other EoC simulations, when compared to the historical
625 counterpart the EoC wettest year shows a sharper decline in seasonal above and below groundwater
626 storage changes (occurring between peak flow and baseflow). Groundwater storage decreases 47%
627 in the EoC between peak flow and baseflow, whereas only a 41% decrease occurs in the historical

628 wet WY. Similarly, surface water storage decreases 44% in the EoC whereas only a 41% decrease
629 occurs in the historical wet WY.
630
631 **3.4. Spatial patterns of the changes in fluxes and pressure-heads**
632 **3.4.1. Median water years**
633 To provide a deeper understanding of how the changes in precipitation timing, magnitude,
634 and phase affect the land surface processes and surface and subsurface hydrodynamic responses,
635 we assess the spatial patterns of these changes during two key periods in the WY, peak flow and
636 baseflow. Figure 7 shows the percent changes in *ET*, surface water pressure-heads, and subsurface
637 pressure-heads (i.e., pressure-heads of the model bottom layer) in the EoC median WY compared
638 to the historical median WY during peak flow and baseflow conditions (see the time frames in
639 Figure 6). Regions in red correspond to areas with smaller fluxes or pressure-heads in the EoC
640 compared to the historical ones, whereas regions in blue correspond to areas with larger fluxes or
641 pressure-heads in the EoC compared to the historical median WY. We study peak flow and
642 baseflow conditions because the analysis of the temporal variations of fluxes and storages has
643 shown that these two periods are characterized by different trends and represent the key periods in
644 understanding the hydrologic responses to the EoC extreme climate.
645 Relative to the historical median WY, during peak flow the EoC median WY is
646 characterized by an increased *ET* across the majority of the watershed, especially in the Central
647 Valley, and larger surface water and subsurface pressure-heads (Figure 7a-c). *ET* increases in the
648 EoC both because of the increase in water availability and increased evaporative demand, as
649 discussed in the previous section (3.3.1.). The increase in *ET* is non-uniform across the watershed
650 because of the heterogeneity of the landscape's topographical gradients, land-surface cover, and

651 subsurface geological conditions. The Central Valley is characterized by a large increase in *ET*
652 compared to the Sierra Nevada, and the patterns of *ET* in the Central Valley are also more
653 homogeneous, a resultant of the geological characteristics of the area and the hydroclimate of the
654 watershed (i.e., where most of the precipitation falls over the Sierra Nevada but follows
655 topographic gradients downward into the valley where more recharge occurs). This leads to more
656 water available in the Central Valley compared to the Sierra Nevada characterized by less
657 permeable rocks. In addition, as most of the *ET* in the Central Valley comes from evaporation due
658 to the high temperatures of the EoC (not shown here), the increase in evaporation is higher in the
659 Central Valley due to its aquifers characterized by a high permeability (Maina and Siirila-
660 Woodburn, 2020) and the availability of water.

661 Surface and subsurface pressure heads both show general increases during the EoC peak
662 flow, yet these maps reveal that unlike *ET* the pressure head (and therefore storage) of water is
663 very heterogeneous in space. For example, in the Sierra Nevada, we observe an increase in
664 subsurface pressure-head (Figure 7c) only in some relatively permeable areas susceptible to
665 infiltration and recharge. Although the Central Valley aquifers are more permeable and
666 geologically less heterogeneous than the Sierra Nevada (as defined in the model), the changes in
667 subsurface pressure-head in the Central Valley are heterogeneous. This is because the recharge of
668 the Central Valley aquifers is dependent on the subsurface and surface flows from the headwater
669 (i.e., connectivity to the headwater). In other words, only areas of the Central Valley that are
670 subject to stronger connectivity with the headwaters see an increase in subsurface pressure-head
671 in the EoC, likely because they are more regularly recharged by the headwaters through surface
672 and subsurface flows from these areas, a recharge that buffers the water depletion through *ET*.

These are mostly the areas located close to the streams where there is an exchange between the subsurface and the surface and the Sierra Nevada foothills (in the alluvium 3 area, see Figure 1).

Relative to its historical counterpart, the EoC median WY is characterized by high *ET* during baseflow conditions though less than during peak flow conditions. (Figure 7d). We observe larger surface water pressure-heads in higher-order streams whereas surface water pressure-heads decrease in the EoC in the majority of the low-order, ephemeral streams (Figure 7e). This opposition of spatial pattern trends, resulting in more water in the main river channels, and less in the smaller streams, occurs for several reasons. First, peak flow occurs earlier in the EoC and is more rainfed, so that the ephemeral streams drain earlier in the EoC compared to in the historical period. This sustained and longer duration of draining increases the surface water pressure-head along the main river channels and is due to the contribution of the subsurface in the headwaters. This contribution is also higher in the EoC due to larger amounts of precipitation. The trends along the main river channel are also evident in the subsurface pressure-head maps (Figure 7f). Because the surface water is larger along the main channels, the subsurface pressure-heads are also larger here due to the interconnection between the subsurface and the surface (Figure 7f). However, in general, subsurface pressure-heads decrease elsewhere in the EoC during baseflow because of the lack of snowmelt and the higher *ET* demand. This result highlights the spatiotemporal complexity of an expected watershed's response to changes in climate (shown here to be bi-directional), and how factors such as river proximity may be crucial for consideration.

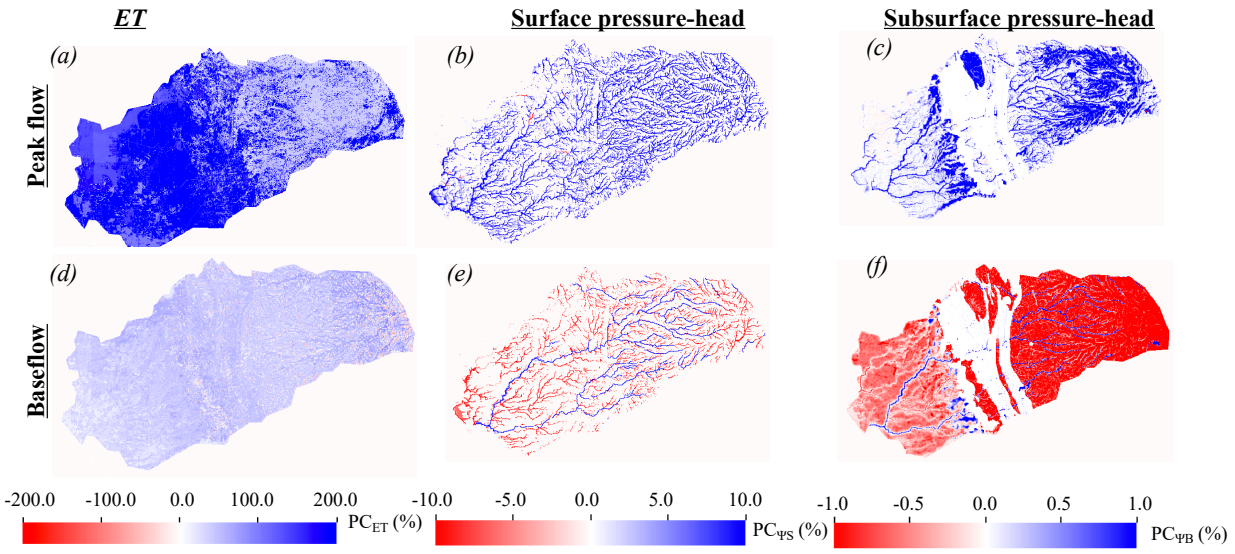

Figure 7: Comparisons between EoC median water year (WY) and the historical median WY peak flow and baseflow spatial distributions of percent changes in *ET* (PC_{ET}), surface water ($PC_{\Psi S}$) and subsurface ($PC_{\Psi B}$) pressure-heads. Regions in red correspond to areas with smaller fluxes or pressure-heads in the EoC compared to the historical ones, whereas regions in blue correspond to areas with larger fluxes or pressure-heads in the EoC compared to the historical WY.

3.4.2. Dry water years

Figure 8 illustrates the percent changes in *ET*, surface water, and subsurface pressure-heads in the EoC dry WY compared to the historical dry WY during peak flow and baseflow conditions. During peak flow conditions, the EoC dry WY has larger *ET*, surface, and subsurface pressure-heads than the historical dry WY (Figure 8a-c). *ET* is larger in this EoC dry WY not only because it is hotter, but also because there is more precipitation, as noted previously. Increases in surface pressure-heads are non-uniform across the domain. For example, surface water does not increase in high elevation areas (i.e., elevation > 2000m) in the EoC dry WY because the change in the precipitation phase is not significant. The main difference between the EoC and the historical dry

WY is the amount of the water flowing down gradient, which is higher in the EoC, hence the surface water in the EoC becomes higher downstream. The increase in subsurface pressure-heads in the EoC dry WY during peak flow conditions is heterogeneous with patterns similar to the changes in subsurface pressure-heads associated with the EoC median WY.

During baseflow conditions, even though *ET* increases in the EoC driest WY relative to the historical driest WY, surface, and subsurface pressure-heads also generally increase (Figure 8d-f). Given wetter conditions in the driest EoC WY, first-order streams are more pronounced. A few low-order streams have less surface water in the EoC when compared to the historical dry WY, similar to the results of the median WYs (see section 3.4.2). Subsurface pressure-head is generally larger in areas subject to strong connectivity with the headwaters (i.e., receiving more water from the headwaters through subsurface and surface flows) in the EoC dry WY relative to the historical dry WY, with some regions experiencing no change from the historical conditions. This suggests that the larger amount of precipitation associated with the EoC dry WY is sufficient to supply enough water to account for high *ET* demands and recharge the groundwater.

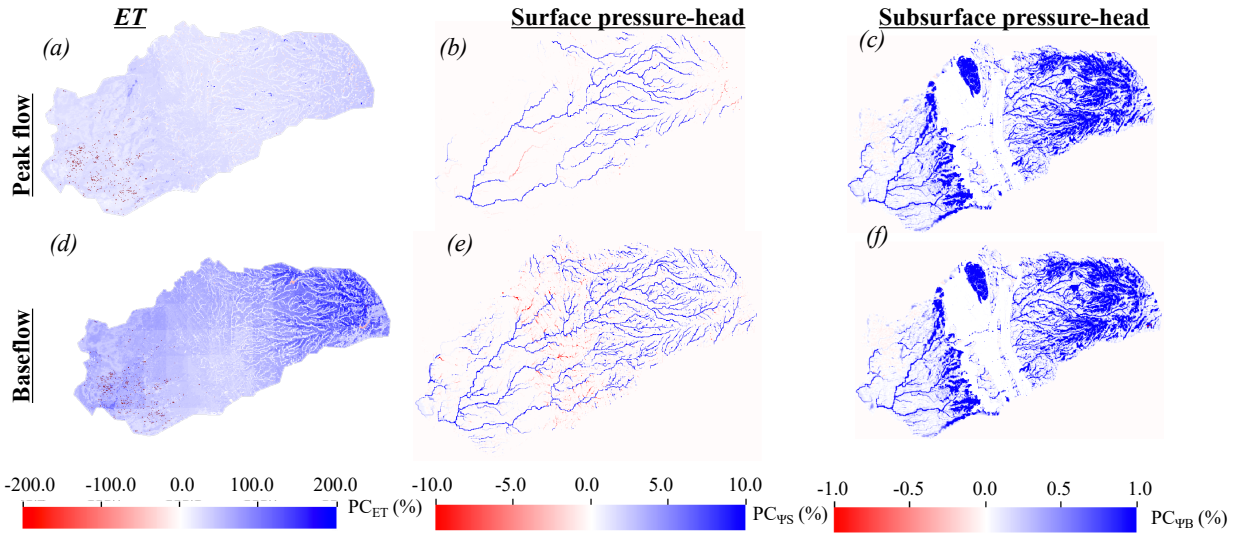

Figure 8: Comparisons between EoC dry water year (WY) and the historical dry WY peak flow and baseflow spatial distributions of percent changes in *ET* (PC_{ET}), surface water ($PC_{\Psi S}$) and

subsurface ($PC_{\Psi B}$) pressure-heads. Regions in red correspond to areas with smaller fluxes or pressure-heads in the EoC compared to the historical ones, whereas regions in blue correspond to areas with larger fluxes or pressure-heads in the EoC compared to the historical WY.

3.4.3. Wet water years

Figure 9 shows the percent changes in *ET*, surface water, and subsurface pressure-heads in the EoC wet WY compared to the historical wet WY during peak flow and baseflow conditions. During peak flow, the EoC wet WY is characterized by larger *ET* and subsurface pressure-heads relative to the historical wet WY and a more heterogeneous mixture of regions with both higher and lower surface water conditions throughout the catchment (Figure 9 a-c). Analogous to other WYs at EoC, the surface water pressure-head increases (decreases) are apparent in larger-order (smaller order) streams, both in the Sierra Nevada and in the Central Valley. In the wettest WY, this occurs for several reasons. First, the larger volume of precipitation, plus seasonal shifts in precipitation timing result in the filling of the higher-order streams and depletion of the lower-order streams during peak flow. Second, in the historical wet WY, a significantly greater amount of snowpack is present in the Sierra Nevada in the upper elevation of the headwaters, allowing for slower, steadier amounts of water that is released during the spring via snowmelt, and in turn, supporting low-order streams over a longer period of time. The latter effect is immediately visible in Figure 9e, where decreases in EoC surface pressure heads are visible in the headwaters, despite the watershed-total showing an increase in EoC surface water storage during baseflow (see Figure 6). Similar to the two previous EoC WYs, the subsurface pressure-head increases are shown more distinctly in the Central Valley during peak flow, under the main river channels, and in the foothills during baseflow (see previous sections on the discussion of hydroclimatic and geologic impacts).

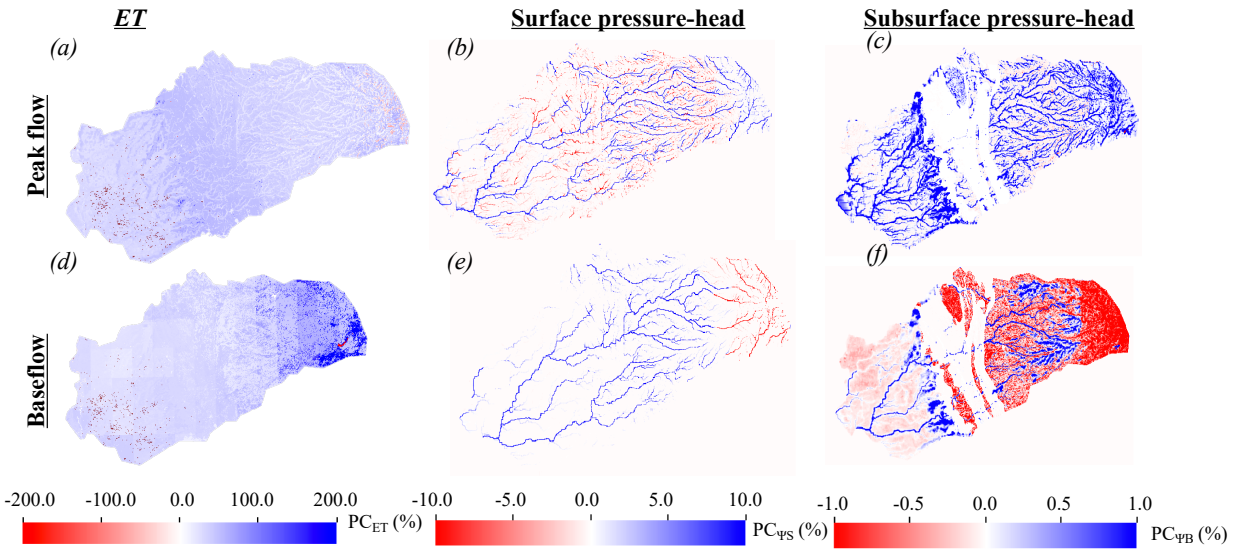

Figure 9: Comparisons between EoC wet water year (WY) and the historical wet WY peak flow and baseflow spatial distributions of percent changes in *ET* (PC_{ET}), surface water ($PC_{\Psi S}$) and subsurface ($PC_{\Psi B}$) pressure-heads. Regions in red correspond to areas with smaller fluxes or pressure-heads in the EoC compared to the historical ones, whereas regions in blue correspond to areas with larger fluxes or pressure-heads in the EoC compared to the historical WY.

4. Discussion

4.1 Comparison with previous studies

Some of the results presented in this study are qualitatively in agreement with previous studies yet provide important new insights. For example, Maurer & Duffy, (2005) used 10 global climate models to predict, as in this study, an increase in winter flows with an earlier peak flow timing in the WY and a decrease in summer flows. Maurer & Duffy show that mid-century projected annual precipitation and streamflow increases of 7% and 13% (respectively). Although our study focused on EoC projections, we found that compared to the historical median WY, annual surface water will increase by 19% in the EoC median WY. Compared to their findings,

764 our work sheds light on how these changes in runoff will occur across the watershed based on its
765 physical characteristics and highlights that while runoff will increase in the EoC lower-order
766 streams mainly located in the Sierra Nevada will see a decrease due to the change in the
767 precipitation phase. Mallakpour et al., (2018) also had a similar finding in a study that shows that
768 future California streamflow is altered similarly to Maurer & Duffy, (2005) under both the RCP4.5
769 and RCP8.5 emissions scenarios, with RCP8.5 showing the highest changes during peak flow.
770 However, contrary to our work the authors mentioned that the annual changes in streamflow will
771 not be significant probably due to the compensation between increases in peak flow and decreases
772 in baseflow. This was likely shaped by the differences in climate and hydrologic models used to
773 derive these conclusions. Similar changes in streamflow were obtained by He et al., (2019) who
774 drove the hydrologic model VIC with 10 global climate models to understand potential changes in
775 runoff in California due to climate change. Hydrologic changes computed from the 10 global
776 climate models were consistent and robust and showed an increase of around 10% in annual
777 streamflow by the late century, a percentage similar to what has been found in this study. The
778 authors mentioned that watershed characteristics such as geology, topography, and land cover
779 strongly impact the hydrologic response to climate change. Relationships between watershed
780 characteristics (e.g., physiographic parameters) and its responses to climate change were further
781 explored by Son & Tague, (2019) who highlighted that because vegetation and subsurface geology
782 control both water availability and energy demand, they in turn influence watershed sensitivity to
783 a changing climate as shown in this study.

784 The increases in groundwater storage shown in this study are also in agreement with
785 Niraula et al., (2017) who used the hydrologic model VIC to show that groundwater recharge will
786 likely increase in the northern portion of the western United States in a changing climate. However,

787 contrary to their work that estimates changes in groundwater recharge over a large domain (i.e.,
788 the western United States). In this work, we show that groundwater recharge decreases in the
789 summer in some areas due to the lack of snowmelt and high EoC *ET*. Increases in *ET* in response
790 to global warming were also documented by Pascolini-Campbell et al., (2021) who showed a 10%
791 increase in global *ET* from 2003 to 2019.

792 An advantage of our approach is a more explicit estimate of spatiotemporal changes in
793 groundwater-surface water feedbacks because Parflow-CLM physically solves the transfer and
794 movement of water from the bedrock to the canopy. Additionally, the aforementioned studies used
795 different emission scenarios and models to project changes in hydrology, nonetheless, their results
796 have shown that the directions of the observed changes are consistent across models and emission
797 scenarios and only the magnitude of these changes is uncertain. Hence, the trends observed in this
798 study using a single model and emission scenario likely represent the trends we would observe
799 using different models and scenarios. While our results show similar patterns and changes, our
800 study provides a much finer-grained perspective on the sensitivity of a watershed to changes in
801 climate extremes based on its subsurface geology, topography, and land cover. It also highlights
802 that the spatiotemporal analyses of these changes may reveal different trends than if only assessed
803 as annual changes. Understanding these localized changes and sensitivities is critical and has
804 practical implications for water management.

805

806 **4.2 Implications for water resources management**

807 Because our work provides a better understanding of the spatiotemporal changes in
808 hydrodynamics in response to future extremes, our findings also have important implications for
809 water resources in California. While previous work more broadly focused on how temperature

increases will alter the precipitation phase and reduce seasonal snowpack and increase winter runoff, this work brings new physical and more granular insights into how watersheds may respond to climate extremes. In particular, both wet and dry WYs in the future experience increased precipitation. As such, even in future dry WYs, water managers and stakeholders may need to prepare more for large precipitation events that may increase the possibility of flooding and require new infrastructure management strategies. For example, in a future where WYs are generally wetter, having alternatives for water supply during periods of sustained drought could be less important. However, as we show in this paper, shifts in precipitation timing, phase, and magnitude have cascading impacts on soil moisture profiles and *ET* withdrawals, which subsequently impact discharge and groundwater dynamics. Future shifts in water availability earlier in the year, as well as more dynamic transitions between peak and baseflow conditions (as quantified here), may impose stresses on water distribution, especially those systems already under scrutiny (e.g. those resources over-allocated or facing environmental degradation).

In addition, while these projections show increases in surface water and groundwater storages at watershed-scale, our results also highlight important localized spatiotemporal changes across a watershed, where the assumption of water storage increase does not necessarily hold in all geographic locations (e.g., areas that are not close to the river in the Central Valley). Our study also shows that the decreases in groundwater storage in the Central Valley aquifers are more significant than the decreases in surface water storage during baseflow conditions. This may call for new conveyance infrastructure that can move water from the relatively wetter areas to the drier areas and/or where infiltration can more readily occur. The latter suggests solutions such as Managed Aquifer Recharge (MAR) could become an increasingly important climate change adaptation. Finally, our study also highlights that lower-order streams will likely become more

ephemeral in the EoC due to flashier runoff and higher evaporative demand, such conditions will have important implications for fish spawning and ecosystem nutrient cycling. Although our results are embedded with uncertainties and are based on a single projection and model, they do highlight the need for a revisitation of current water management strategies. Further studies using different climate and land-use scenarios and models of varying complexity and resolution could help build more confidence and provide more information in defining how future water management strategies would need to change to be more resilient to more extreme WYs in the future.

4.3 Study limitations

This study combines novel climate and hydrologic simulations that provide both advantages and disadvantages compared with previous work (He et al., 2019; Maurer & Duffy, 2005; Niraula et al., 2017; M. Safeeq et al., 2014; Son & Tague, 2019). We note several of these disadvantages below. In the integrated hydrologic model, the subsurface geology and land cover characterization has inherent and, in some cases, irreducible uncertainty. This study uses hydrodynamic parameters as defined by Maina et al. (2020a), which assumes that the subsurface hydrodynamics from the Sierra Nevada to the Central Valley is almost completely hydrologically separated except through overland flow. However, it is not clear whether fractures or other macrostructures may drive more surface and subsurface flows from the headwaters to the Central Valley aquifers. In addition, we use the historical land surface cover map when simulating the EoC. Since vegetation will dynamically respond to a changing climate, the land surface cover used in the EoC simulations may be unrealistic and may influence, for example, *ET* and/or soil moisture. For example, it has been shown that the stomatal resistance of plants will change due to rising CO_2

with important implications for both the water and energy balance (Lemordant et al., 2018; Milly & Dunne, 2017). Yet, our use of historical land surface cover does have the advantage of isolating changes in fluxes associated with climate change alone and could be compared in future work with additional simulations that account for both changes in the land surface and climate. Future studies will assess the impact of changes in vegetation physiology and land surface cover on watershed hydrodynamics. In this study, we did not include the impacts of anthropogenic activities such as pumping and irrigation due to the uncertainties in predicting these fluxes in EoC. While these human interventions could substantially change the hydrologic system, our study isolates the impacts of a changing climate on the natural system. Future studies can now estimate the impacts of different pumping and irrigation scenarios at EoC that may further impact the hydrologic system hydrodynamics in a changing climate and compare and contrast with this work. Last, although our VR-CESM simulations represent a cutting-edge global climate model simulation (e.g., 28 km regional grid-refinement, coupled atmosphere-land simulation with prescribed ocean conditions, etc.), further work may be needed to evaluate how a more refined grid resolution impacts atmospheric process representation over the Cosumnes watershed, particularly in the headwaters (Maina et al., 2020b). We further acknowledge that the 30-year simulation may not be sufficient to capture certain climate extremes (e.g., 1-in-50-year storm). Future studies, if computational resources are available, will seek to explore how the use of a longer time period might influence the identification of the most extreme dry and wet WYs from VR-CESM.

5 Summary and Conclusions

The effects of climate change are increasingly felt across many regions of the world, especially in hydrologically sensitive regions with Mediterranean climates such as California.

879 Many studies over the years have been conducted to better understand the hydroclimate of the EoC
880 and its impacts on the hydrologic cycle. Previous studies have used a multitude of different models
881 at varying complexity and climate scenarios to highlight that the future climate has multiple
882 plausible outcomes. Most of these studies indicate warmer temperatures and precipitation that
883 mostly falls as rain instead of snow. For example, the state of California is projected to experience
884 more punctuated climate extremes coupled with a marked decrease in the Sierra Nevada snowpack
885 (Cayan et al., 2008; Gleick, 1987; Musselman, Molotch, et al., 2017; Rhoades, Ullrich, &
886 Zarzycki, 2018). Such drastic transitions have already started to shape the hydroclimate of
887 California. Faced with this new normal, it is becoming increasingly important to assess how the
888 integrated hydrologic cycle may respond to these perturbations and connect these responses more
889 directly to water resource management, particularly with modeling frameworks that can better
890 represent the interactions between the changing atmosphere and the surface and subsurface
891 hydrology.

892 In this work, we used state-of-the-art physics-based models at high resolutions for their
893 respective communities to project changes in meteorological conditions at the EoC and assess how
894 their combined effects influence watershed hydrology from the land surface to the deeper
895 subsurface. Importantly, our approach to couple a variable resolution Earth System Model and an
896 integrated hydrologic model allow for us to simulate hydro-meteorological conditions which are
897 jointly driven by thermodynamical and dynamical shifts in climate. We model the Cosumnes
898 watershed, which spans the Sierra Nevada and Central Valley and hosts one of the last rivers in
899 the state without a large dam, as a testbed to understand how climate drivers will impact water
900 resources in the EoC. We performed climate simulations over 30-year periods historically (1985-
901 2015) and at EoC (2070-2100) and identified the driest, median, and wettest WYs from those

902 simulations, which were then used as meteorological forcing for the hydrologic model. Our
903 coupled simulations project that, for the Cosumnes watershed, temperature and precipitation will
904 both increase by the EoC across all WY types (wettest, median, and driest). In addition,
905 precipitation is projected to fall earlier compared to historical conditions and mainly in the form
906 of rain. For the median and wet WYs the precipitation season has earlier cessation dates, while the
907 dry EoC WY, which is wetter than its historical counterpart, persists significantly longer into the
908 spring. As a consequence of warmer temperatures, all WYs show a substantial decrease in *SWE*.
909 The shift of precipitation from snowfall to rainfall, as well as the increase in the amount of
910 precipitation and the early start of precipitation lead to an overall increase in soil moisture and
911 more water available to meet the higher EoC *ET* demand. Importantly, this increase in *ET* is
912 heterogeneous across the watershed and highlights one of the main advantages of using an
913 integrated hydrologic model such as the one we employed in this study to assess the spatiotemporal
914 patterns of change. Our results show that the sensitivity to the changes in *ET* at EoC depends on
915 the subsurface geology and topographical gradients. More specifically:

916 - The geological and topographical complexities of the Sierra Nevada headwaters
917 lead to highly heterogeneous changes in *ET*. Changes in *ET* are higher in permeable
918 areas such as the plutonic rocks where water can be more easily extracted.
919 - *ET* changes in the Central Valley of the Cosumnes watershed are predominantly
920 uniform with the highest sensitivities in the vicinity of the Cosumnes River due to
921 the high availability of water.

922 Precipitation increases enough in the EoC to provide water for both increased *ET* and
923 increased surface water storage. Surface water storages also increase earlier in the WY and have
924 higher peak amounts. This earlier and larger increase is a direct consequence of an earlier start in

925 precipitation at EoC, a marked change in the precipitation phase, and an overall larger amount of
926 precipitation when compared with the historical WYs. However, our results also highlight that
927 during baseflow conditions surface water decreases, especially in lower-order streams, showing
928 that these areas are highly sensitive to the change in precipitation phase. Our simulations also show
929 that the seasonal variability of the EoC watershed behavior is also more dynamic. In general,
930 decreases in seasonal water storages occurring between peak flow and baseflow conditions are
931 more than 10% higher in the EoC compared to the historical conditions.

932 EoC groundwater storages are also projected to increase earlier in the WY with peaks
933 greater than those found historically. Yet these storages decrease significantly during baseflow
934 conditions due to the higher *ET* at EoC and the absence of recharge from snowmelt. Contrary to
935 the changes in surface water storages, groundwater storages show a larger decrease due to their
936 dependence on the surface water from the Sierra Nevada. Our results also show that changes in
937 subsurface pressure-heads are not uniform and are bi-directional throughout the Cosumnes
938 watershed. Because the connectivity between the Central Valley aquifers and the Sierra Nevada
939 headwaters (i.e., subsurface and surface flows from the headwater to the Central Valley aquifers)
940 plays an important role in the hydrodynamics of this watershed, only areas with a strong connection
941 with the headwaters, such as the foothills and the river channels, see an increase in subsurface
942 pressure-heads at EoC. However, the subsurface pressure-heads decrease elsewhere in the Central
943 Valley aquifers especially in baseflow conditions due to the high *ET* and the lack of snowmelt. In
944 the river channels, this is due to the exchange between the subsurface and the surface whereas the
945 foothills characterized by the consolidated sediments serve as “spillover.”

946 Our results provide novel understandings about possible changes in the integrated
947 hydrologic response to changes in EoC climate extremes. An important caveat is that our

948 simulation was a single set of climate realizations and may not properly bound internal variability
949 uncertainty like an ensemble of climate simulations could. However, beyond the widely agreed-
950 upon changes of decreased snowpack and shifts in runoff timing in the literature, we show that in
951 this simulation: 1) EoC precipitation increases even in the driest years; 2) despite an increased
952 temperature, and hence *ET*, both groundwater and surface water storage increase relative to
953 historical conditions because of increased precipitation; and 3) there is a distinct spatial pattern,
954 particularly in surface water storage, in which smaller-order streams see reduced flow while the
955 larger order streams see an increased flow. These changes will have strong implications on natural
956 resource management.

957 In this study, land cover changes are assumed to not occur, however, changes in land cover
958 are expected to occur in the future, either naturally or anthropogenically. Further vegetation
959 physiology will also change in response to an increase in CO_2. Thus, future studies should
960 investigate the impacts of these changes and how they may further alter the integrated hydrologic
961 budgets. Additionally, future studies could also assess the effects of anthropogenic activities such
962 as pumping and irrigation under a changing climate, other emissions scenarios, and/or the
963 sequencing of variable end-member WYs and the interannual memory of the hydrologic system.
964 Importantly, an understanding of this variability could be used to inform how water managers
965 might prepare for more intense and/or intermittent extremes in the future. Future research could
966 also use multiple emission scenarios to better assess the range in hydrodynamic responses
967 dependent on the severity of climate change, especially those related to the magnitude and spatial
968 location of the precipitation response since they are likely more uncertain and scenario-dependent
969 than the trends at the watershed-scale.

Appendix A: Comparisons between VR-CESM and PRISM historical conditions

Figure A1 highlights differences in dry, median, and wet WY accumulated precipitation relative to the 1981-2019 PRISM climatology. VR-CESM generally recreates the spatial pattern of anomalous dry and wet patterns across California for each WY type. This is shown via the common regions of minimum and maximum anomalies relative to the PRISM climatology. Notably, there are regions where VR-CESM anomalies are not consistent with PRISM. This is primarily shown in the wettest water year in portions of the Central Valley, western slopes of the Sierra Nevada, and southern California. This is likely correlated with resolution and the lack of orographic gradients (both valleys and peaks) in VR-CESM at 28km resolution. Mismatches in accumulated precipitation may also be due to representation of atmospheric rivers (ARs) in VR-CESM that were found to be generally larger, slightly more long-lived and make landfall more frequently over California (Rhoades et al., 2020b). Figure A2 shows Cosumnes watershed WY accumulated precipitation and surface temperature. WY accumulated precipitation is shown in Figure A 2a and 2b for PRISM and VR-CESM, respectively. All WY accumulated precipitation simulated by VR-CESM over 1985-2015 are within the range in PRISM, save for the wettest WY. This is shown more explicitly in quadrant space in Figure A2c where the range of annual bias in VR-CESM relative to the range of interannual variability in PRISM for accumulated precipitation and temperature is shown. VR-CESM generally simulates a wetter historical period over the Cosumnes (range of bias of 1330 mm) relative to PRISM (range of interannual variability of 1320 mm). Basin-average minimum (421 mm) and maximum (1740 mm) WY accumulated precipitation are slightly larger than is found in PRISM. Of relevance to this study, PRISM has shown notable uncertainties in the Sierra Nevada. Lundquist et al., 2015 showed that an underrepresentation of the most extreme storm total precipitation in the Sierra Nevada can result

993 in an upper-bound uncertainty of 20% in WY accumulated precipitation. Therefore, the wettest
994 WY of VR-CESM is well within the 20% uncertainty range of PRISM's wettest WY (1580 ± 316
995 mm). Further, differences in basin-average WY accumulated precipitation between VR-CESM
996 and PRISM are non-significant using a t-test and assuming a p-value < 0.05. The range of
997 temperature bias in VR-CESM (2.74 °C) relative to the range of PRISM interannual variability
998 (2.93 °C) was also within the temperature uncertainties discussed in Strachan and Daly, 2017.
999 They showed that a general cool-bias in PRISM temperatures were found on the leeside of the
1000 Sierra Nevada when compared with 16 out-of-sample in-situ observations across an elevation
1001 gradient of 1950 to 3100 meters with an overall mean bias of −1.95 °C (maximum temperature)
1002 and −0.75 °C (minimum temperature).

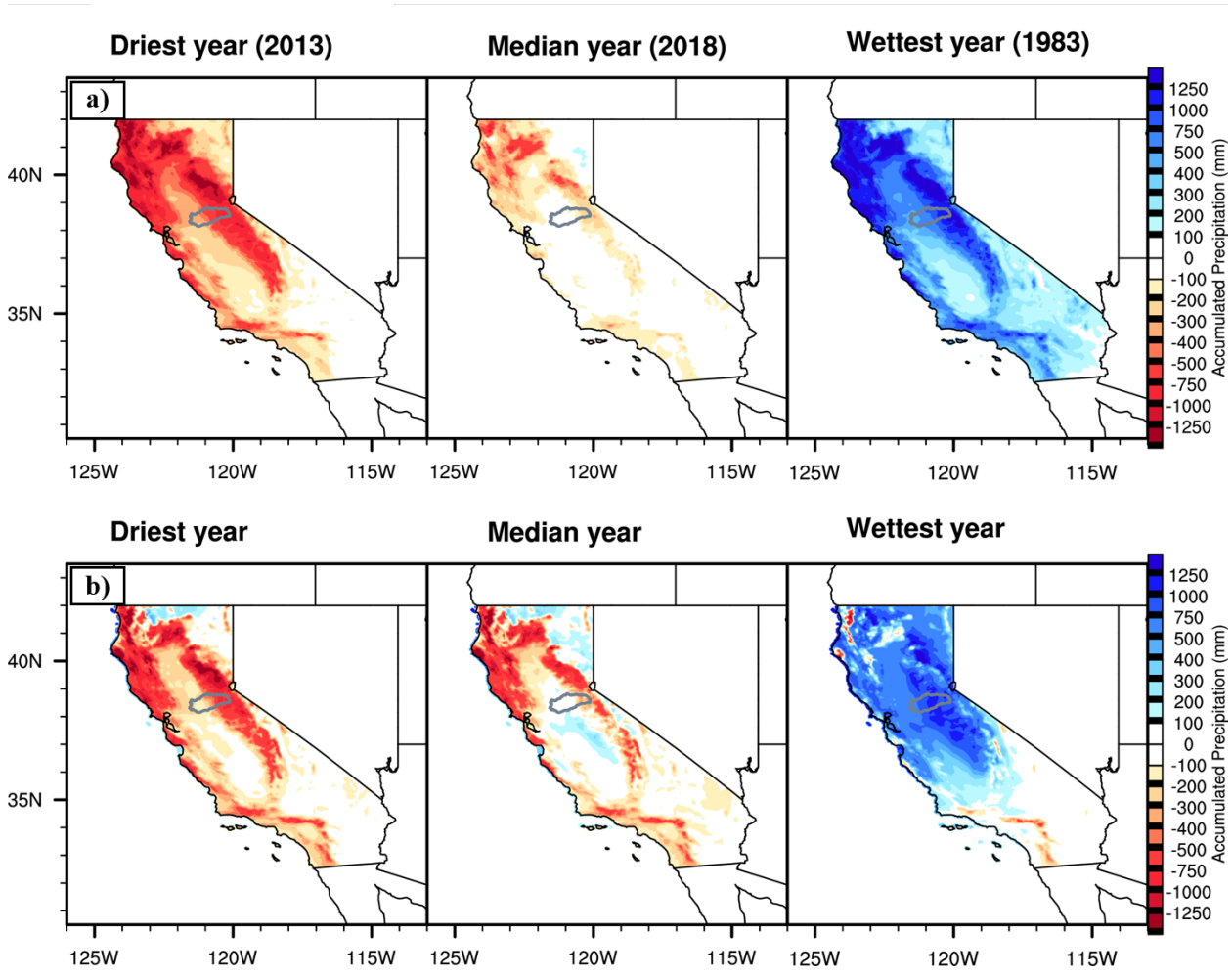

1003

Figure A1: Differences in the driest, median, and wettest water year accumulated precipitation over California in a) PRISM and b) VR-CESM relative to the 1981-2019 PRISM climatology. The Cosumnes watershed boundary is outlined in gray.

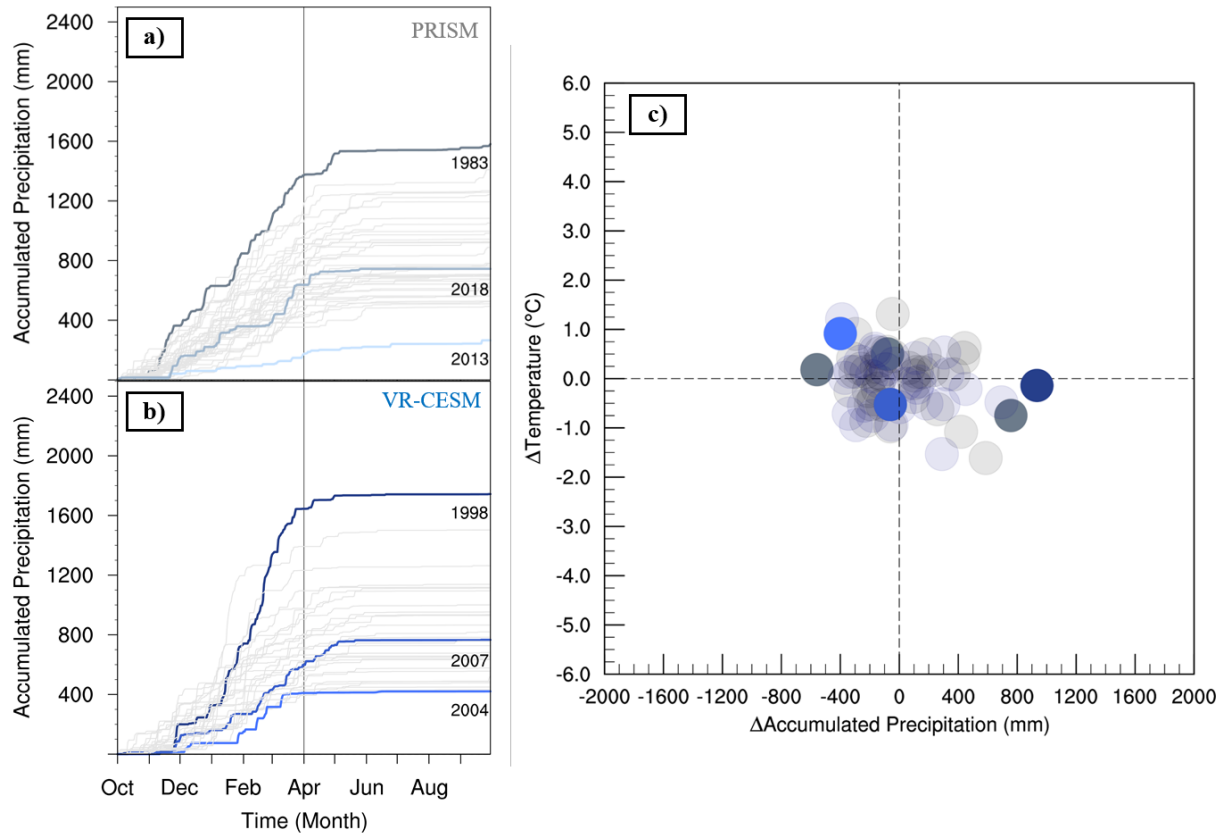

Figure A2: Cosumnes watershed accumulated precipitation totals in a) PRISM (gray; 1981-2019) and b) VR-CESM (blue; 1985-2015) with dry, median, and wet years emboldened. c) shows differences in PRISM (gray) and VR-CESM (blue) relative to the PRISM climatology (1981-2019) in temperature and accumulated precipitation quadrant space. Dry, median, and wet water years are emboldened.

Appendix B: Integrated Hydrologic Model Parameterization

1. Input Variables

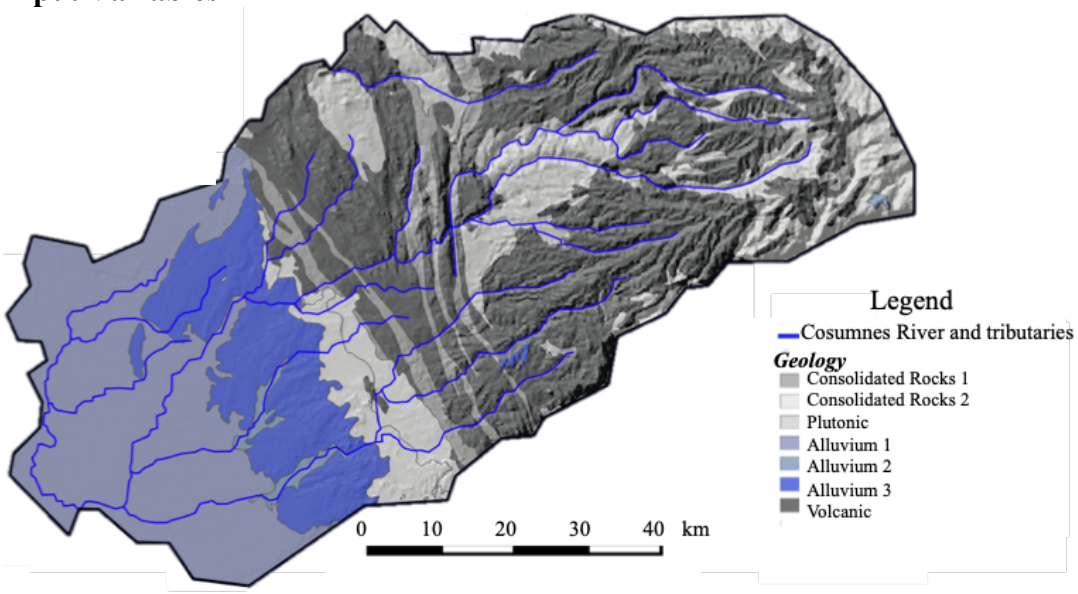

Figure B1: Geological map of the Cosumnes watershed (source: USGS, Jennings et al., 1977)

Hydrodynamic properties based on the geology				
Geological Formation	Porosity (-)	Specific Storage (m^{-1})	Van Genuchten α (m^{-1})	Van Genuchten n (-)
Bedrock (Consolidated, Plutonic and Volcanic Rocks)	0.02	10^{-6}	3.0	3.0
Alluvial aquifers	0.2	10^{-4}	3.0	3.0

Table B1: Assigned values of hydrodynamic parameters (porosity, specific storage and Van Genuchten parameters). Values are based on literature review (Faunt et al., 2010; Faunt and Geological Survey (U.S.), 2009; Flint et al., 2013; Gilbert and Maxwell, 2017; Welch and Allen, 2014).

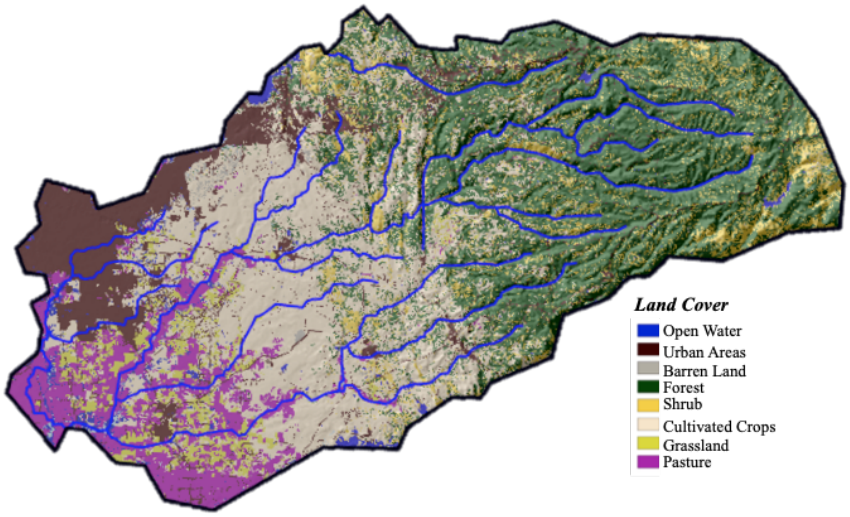

Figure B2: Cosumnes watershed characteristics: land use and land cover (source: Homer et al., 2015), and model boundaries.

	Surface roughness based on land use			
Land Use		**Manning Coefficient ($h.m^{-1/3}$)**		
Forest		$5x10^{-2}$		
Shrub land and agricultural area		$5x10^{-3}$		
Urban areas		$5x10^{-5}$		
	Crop properties			
	Crop Type and Reference	**Height (m)**	**Maximum Leaf Area Index (-)**	**Minimum Leaf Area Index (-)**
	Alfalfa (Evett et al., 2000; Orloff, 1995; Robison et al., 1969)	0.6	6.0	2.0
	Pasture (Buermann et al., 2002; King et al., 1986; Rahman and Lamb, 2017)	0.12	6.0	1.0
	Vineyards (Johnson and Pierce, 2004; Vanino et al., 2015)	0.9	3.0	0.6

Table B2: Manning coefficients and crop properties

Boundary conditions	**Value**
Mokelumne and American river	Weekly-varying Dirichlet boundary conditions. These values are based on the measured river stages.
Sierra Nevada limit	No flow Neumann boundary condition
Bottom of the model	No flow Neumann boundary condition

Table B3: boundary conditions

2. Numerical model set-up

<table>
<tr><td>Domain size</td><td>~7000 km^2</td></tr>
<tr><td>Spatial discretization</td><td>200 m horizontal from 0.1 m to 30 m in the vertical direction
<table><tr><td colspan="9">Vertical Resolution</td></tr><tr><td>Layer</td><td>1</td><td>2</td><td>3</td><td>4</td><td>5</td><td>6</td><td>7</td><td>8</td></tr><tr><td>Δz(m)</td><td>0.1</td><td>0.3</td><td>0.6</td><td>1.0</td><td>8.0</td><td>15.0</td><td>25.0</td><td>30.0</td></tr></table></td></tr>
<tr><td>Simulation time</td><td>Model validation (from water year 2012 to water year 2017), then future water years</td></tr>
<tr><td>Temporal discretization</td><td>hourly</td></tr>
</table>

Table B4: Numerical model discretization

3. Output variables

Selected output variables	**Temporal scale**	**Spatial scale**
Snow Water Equivalent	Yearly, monthly, and hourly	Domain-average and point scale
Evapotranspiration	Yearly, monthly, and hourly	Domain-average and point scale
Soil Moisture	Yearly, monthly, and hourly	Domain-average and point scale
River Stages (also surface water storages)	Yearly, monthly, and hourly	Domain-average and point scale
Groundwater levels variations (also subsurface storages)	Yearly, monthly, and hourly	Domain-average and point scale

Table B5: Selected output variables

Appendix C: Integrated Hydrologic Model Validation

We compared temporal variations of streamflow at 3 stations located in the Sierra (uplands), the intersection between the Sierra and the Central Valley, and the outskirts of Sacramento (see Figure C1). Four wells in the watershed (see Figure C1) have reasonable, publicly available records of groundwater levels and were used to check the ability of the model to reproduce water table depth variations.

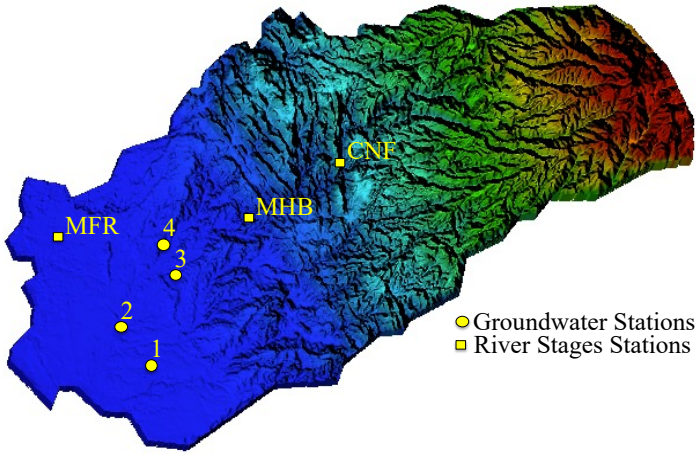

Figure C1: The locations of the 3 streamflow gauges (CNF, MHB, and MFR) and 4 groundwater wells (stars).

Figure C2a depicts the comparisons between simulated and measured river stages at the 3 stations indicated in figure C1. Absolute errors (L1) in m and relative errors (L2) are shown in Table C1. Differences between simulated and measured streamflow vary between 0.4 and 0.8 m (Table C1) indicating that the model is able to reproduce the river dynamics.

Absolute differences given by:

$$L_{1_{i,j}} = \left| X_{mes_{i,j}} - X_{sim_{i,j}} \right| \quad \text{(C1)}$$

Where $L_{1_{i,j}}$ is the absolute difference associated with cell i and time j, $X_{mes_{i,j}}$ is the measured (or remotely sensed) data, and $X_{sim_{i,j}}$ the simulated value.

Relative differences $L_{2_{i,j}}$ are given by:

$$L_{2_{i,j}} = \frac{|X_{mes_{i,j}} - X_{sim_{i,j}}|}{X_{mes_{i,j}}} \quad \text{(C2)}$$

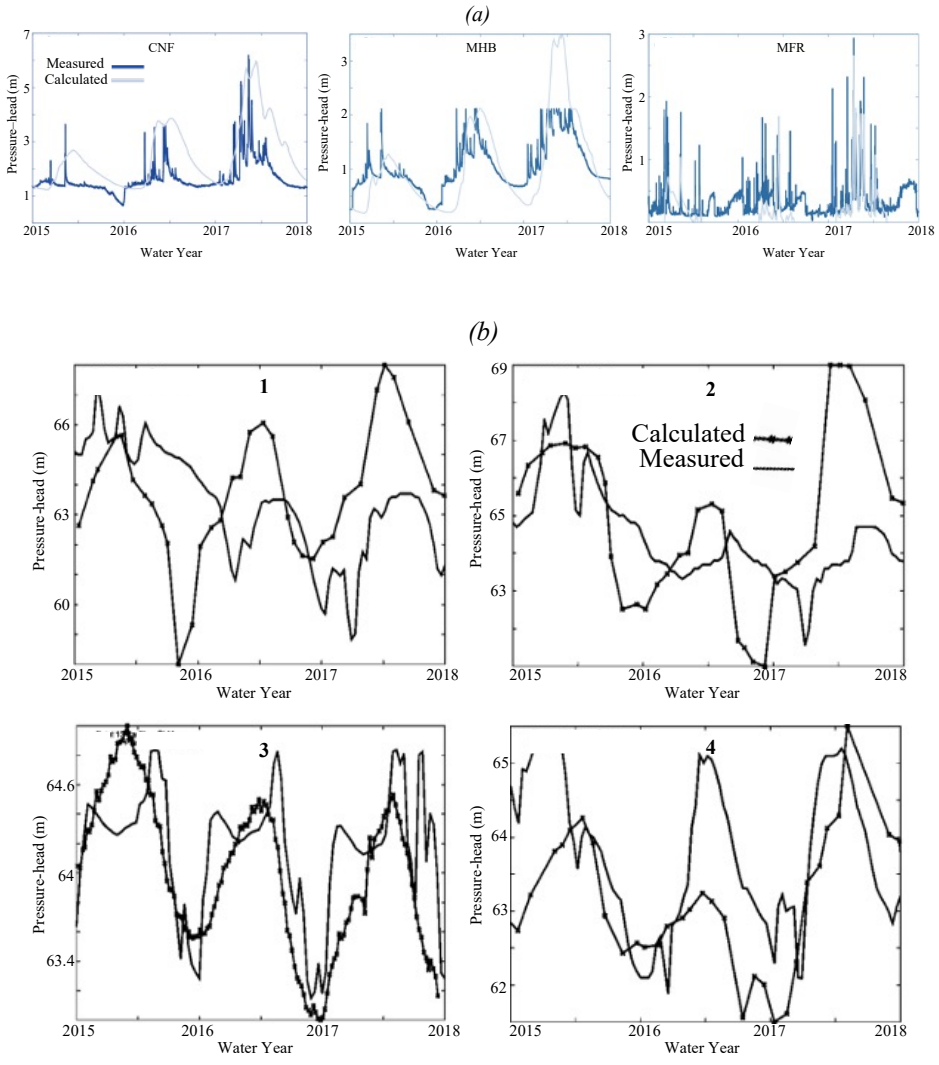

Figure C2: Comparisons between measured and calculated (a) river stages (i.e., pressure-heads simulated by ParFlow-CLM) and (b) subsurface pressure-head. The location of the selected points is indicated in Figure C1.

Measurements	**L_1 (m)**	**L2 (-)**
River Stages (CNF)	0.8	0.5
River Stages (MHB)	0.4	0.36
River Stages (MFR)	0.57	1.06
Groundwater Levels (Well 1)	3.73	0.05
Groundwater Levels (Well 2)	1.63	0.02
Groundwater Levels (Well 3)	0.476	0.0077
Groundwater Levels (Well 4)	1.08	0.016

Table C1: Differences between measured and calculated surface and groundwater levels. L1 is the absolute error and R2 the relative error.

Comparisons between simulated and calculated groundwater levels (here referred to as the pressure-heads at the bottom of the domain) shown in Figure C2b indicate that the model has reasonable agreements with measurements. As shown in table C1, the error varies between 0.47 to 3.73 m depending on the station. Mismatches between simulated and observed groundwater levels at wells 1 and 2 are likely due to an inaccurate estimation of pumping in these areas. The temporal variations of the groundwater levels show an impact of withdrawals but because these withdrawals are hard to estimate the model isn't correctly reproducing these trends.

ParFlow-CLM also solves the key land surface processes governing the transfer of water and energy at the land-atmosphere-soil interface: evapotranspiration, snow dynamics, and soil moisture. In Maina et al., (2020a), rigorous comparisons between the ParFlow-CLM simulated land surface processes and remotely sensed estimates of these variables were conducted (Figure

C3). Table C2 shows the correlation coefficient between ParFlow-CLM results and the various datasets compared.

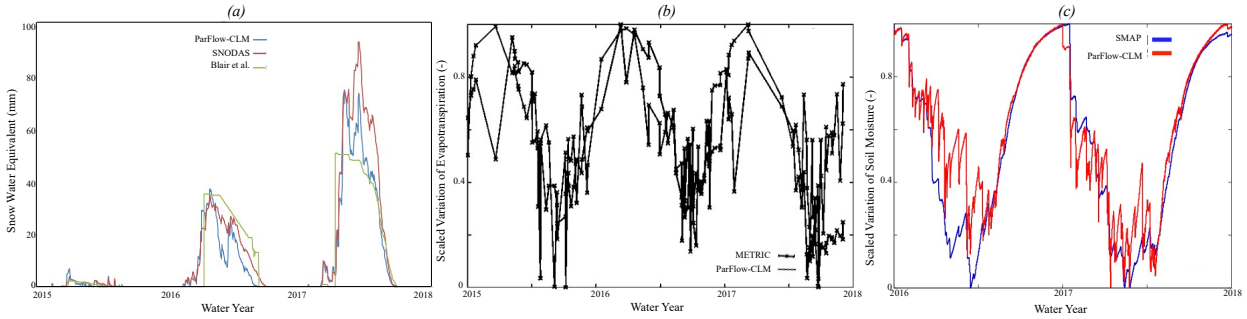

Figure C3: (a) Comparisons between domain-averaged total snow water equivalent obtained with ParFlow-CLM, SNODAS and Bair et al., reconstruction, (b) Comparisons between actual evapotranspiration obtained with ParFlow-CLM and METRIC (c) Relative variation of soil moisture obtained with ParFlow-CLM and SMAP. Note that the x-axis of (c) is shorter because of the availability of SMAP data

Satellites based products	**L_1 (m)**	**L_2 (-)**	**Pearson Correlation Coefficient**
SWE SNODAS (mm)	3.09	3.77	0.97
SWE Bair et al., (mm)	3.80	2.69	0.84
Soil Moisture SMAP (-)	0.217	3.07	0.94
ET METRIC (mm/s)	0.067	1.40	0.6

Table C2: differences between measured and remotely sensed evapotranspiration (METRIC), soil moisture (SMAP), and snow water equivalent (SNODAS and Bair et al., 2016)

Data availability

Data supporting the findings of this study can be found here: https://portal.nersc.gov/archive/home/a/arhoades/Shared/www/Hyperion/

Author contribution

The authors contribute equally to this work.

Competing interests

The authors declare that they have no conflict of interest.

Acknowledgements

Fadji Zaouna Maina and Erica Siirila-Woodburn were supported by LDRD funding from Berkeley Lab, provided by the Director, Office of Science, of the U.S. Department of Energy under Contract No. DE-AC02-05CH11231.

Author Alan M. Rhoades was funded by the Department of Energy, Office of Science Office of Biological and Environmental Research program under Award Number DE-SC0016605 "A framework for improving analysis and modeling of Earth system and intersectoral dynamics at regional scales" and Award Number DE-AC02-05CH11231 “The Calibrated and Systematic Characterization, Attribution, and Detection of Extremes - Science Focus Area”.

This research used computing resources from the National Energy Research Scientific Computing Center, a DOE Office of Science User Facility supported by the http://dx.doi.org/10.13039/100006132 of the U.S. Department of Energy under Contract No. DE-AC02-05CH11231.

References

Abbott, M. B., J. C. Bathurst, J. A. Cunge, P. E. Oconnell, and J. Rasmussen (1986), An introduction to the european hydrological system: Sys- teme hydrologique Europeen, She .2. Structure of a physically-based, distributed modeling system, J. Hydrol., 87(1–2), 61–77.

Allan, R.P., Barlow, M., Byrne, M.P., Cherchi, A., Douville, H., Fowler, H.J., Gan, T.Y., Pendergrass, A.G., Rosenfeld, D., Swann, A.L.S., Wilcox, L.J. and Zolina, O. (2020), Advances in understanding large-scale responses of the water cycle to climate change. Ann. N.Y. Acad. Sci., 1472: 49-75. https://doi.org/10.1111/nyas.14337

Allen R. G., Masahiro T., Ricardo T. (2007)Satellite-based energy balance for mapping evapotranspiration with internalized calibration (METRIC)—model J. Irrig. Drain. Eng., 133, pp. 380-394, 10.1061/(ASCE)0733-9437(2007) 133:4(380).

Alo, C. A., & Wang, G. (2008). Hydrological impact of the potential future vegetation response to climate changes projected by 8 GCMs. *Journal of Geophysical Research: Biogeosciences*, *113*(G3). https://doi.org/10.1029/2007JG000598

Bair E.H., Rittger K., Davis R.E., Painter T.H., Dozier J. (2016) Validating reconstruction of snow water equivalent in California's Sierra Nevada using measurements from the NASA Airborne Snow Observatory Water Resour. Res., 52 , pp. 8437-8460, 10.1002/2016WR018704

Bales, R. C., Molotch, N. P., Painter, T. H., Dettinger, M. D., Rice, R., & Dozier, J. (2006). Mountain hydrology of the western United States. *Water Resources Research*, *42*(8). https://doi.org/10.1029/2005WR004387

1139 Barnett, T. P., Adam, J. C., & Lettenmaier, D. P. (2005). Potential impacts of a warming climate
1140 on water availability in snow-dominated regions. *Nature*, *438*(7066), 303–309.
1141 https://doi.org/10.1038/nature04141
1142 Berghuijs, W. R., Woods, R. A., & Hrachowitz, M. (2014). A precipitation shift from snow
1143 towards rain leads to a decrease in streamflow. *Nature Climate Change*, *4*(7), 583–586.
1144 https://doi.org/10.1038/nclimate2246
1145 Bixio, A. C., G. Gambolati, C. Paniconi, M. Putti, V. M. Shestopalov, V. N. Bublias, A. S.
1146 Bohuslavsky, N. B. Kasteltseva, and Y. F. Rudenko (2002), Modeling groundwater-
1147 surface water interactions including effects of morphogenetic depressions in the Chernobyl
1148 exclusion zone, Environ. Geol., 42(2-3) 162-177.
1149 Cayan, D. R., Maurer, E. P., Dettinger, M. D., Tyree, M., & Hayhoe, K. (2008). Climate change
1150 scenarios for the California region. *Climatic Change*, *87*(1), 21–42.
1151 https://doi.org/10.1007/s10584-007-9377-6
1152 Christensen, L., Tague, C. L., & Baron, J. S. (2008). Spatial patterns of simulated transpiration
1153 response to climate variability in a snow dominated mountain ecosystem. *Hydrological*
1154 *Processes*, *22*(18), 3576–3588. https://doi.org/10.1002/hyp.6961
1155 Collins, W. D., Bitz, C. M., Blackmon, M. L., Bonan, G. B., Bretherton, C. S., Carton, J. A., et al.
1156 (2006). The Community Climate System Model Version 3 (CCSM3). *Journal of Climate*,
1157 *19*(11), 2122–2143. https://doi.org/10.1175/JCLI3761.1
1158 Condon, L. E., Maxwell, R. M., & Gangopadhyay, S. (2013). The impact of subsurface
1159 conceptualization on land energy fluxes. *Advances in Water Resources*, 60, 188–203.
1160 https://doi.org/10.1016/j.advwatres.2013.08.001

1161 Condon, L.E., Atchley, A.L., Maxwell, R.M., (2020). Evapotranspiration depletes groundwater
1162 under warming over the contiguous United States. *Nature Communications* 11, 873.
1163 https://doi.org/10.1038/s41467-020-14688-0
1164 Cook, E. R., Woodhouse, C. A., Eakin, C. M., Meko, D. M., & Stahle, D. W. (2004). Long-Term
1165 Aridity Changes in the Western United States. *Science*, *306*(5698), 1015–1018.
1166 https://doi.org/10.1126/science.1102586
1167 Coon, E. T., J. D. Moulton, and S. L. Painter (2016), Managing complexity in simulations of land
1168 surface and near-surface processes, Environ. Modell Software, 78, 134-149.
1169 Cosgrove, B. A., Lohmann, D., Mitchell, K. E., Houser, P. R., Wood, E. F., Schaake, J. C., et al.
1170 (2003). Real-time and retrospective forcing in the North American Land Data Assimilation
1171 System (NLDAS) project. *Journal of Geophysical Research: Atmospheres*, *108*(D22).
1172 https://doi.org/10.1029/2002JD003118
1173 Cristea, N. C., Lundquist, J. D., Loheide, S. P., Lowry, C. S., & Moore, C. E. (2014). Modelling
1174 how vegetation cover affects climate change impacts on streamflow timing and magnitude
1175 in the snowmelt-dominated upper Tuolumne Basin, Sierra Nevada. *Hydrological*
1176 *Processes*, *28*(12), 3896–3918. https://doi.org/10.1002/hyp.9909
1177 Daly, C., Halbleib, M., Smith, J. I., Gibson, W. P., Doggett, M. K., Taylor, G. H., et al. (2008).
1178 Physiographically sensitive mapping of climatological temperature and precipitation across the
1179 conterminous United States. International Journal of Climatology, 28(15), 2031–2064.
1180 https://doi.org/10.1002/joc.1688.
1181 Dettinger, M. (2011). Climate Change, Atmospheric Rivers, and Floods in California – A
1182 Multimodel Analysis of Storm Frequency and Magnitude Changes1. *JAWRA Journal of*

the American Water Resources Association, *47*(3), 514–523. https://doi.org/10.1111/j.1752-1688.2011.00546.x

Dettinger, M., & Anderson, M. L. (2015). Storage in California's reservoirs and snowpack in this time of drought. *San Francisco Estuary and Watershed Science*, *13*(2). https://doi.org/10.15447/sfews.2015v13iss2art1

Dettinger, M., Redmond, K., & Cayan, D. (2004). Winter Orographic Precipitation Ratios in the Sierra Nevada—Large-Scale Atmospheric Circulations and Hydrologic Consequences. *Journal of Hydrometeorology*, *5*(6), 1102–1116. https://doi.org/10.1175/JHM-390.1

Dettinger, M. D. (2013). Atmospheric Rivers as Drought Busters on the U.S. West Coast. *Journal of Hydrometeorology*, *14*(6), 1721–1732. https://doi.org/10.1175/JHM-D-13-02.1

Di Liberto, T. (2017, October). Very wet 2017 WY ends in California. *NOAA Climate.Gov*. Retrieved from https://www.climate.gov/news-features/featured-images/very-wet-2017-water-year-ends-california

Dierauer, J. R., Whitfield, P. H., & Allen, D. M. (2018). Climate Controls on Runoff and Low Flows in Mountain Catchments of Western North America. *Water Resources Research*, *54*(10), 7495–7510. https://doi.org/10.1029/2018WR023087

Faunt, C.C., Belitz, K., Hanson, R.T., 2010. Development of a three-dimensional model of sedimentary texture in valley-fill deposits of Central Valley, California, USA. Hydrogeology Journal 18, 625–649. https://doi.org/10.1007/s10040-009-0539-7

Faunt, C.C., Geological Survey (U.S.) (Eds.), 2009. Groundwater availability of the Central Valley Aquifer, California, U.S. Geological Survey professional paper. U.S. Geological Survey, Reston, Va.

Ficklin, D. L., Luo, Y., & Zhang, M. (2013). Climate change sensitivity assessment of streamflow and agricultural pollutant transport in California's Central Valley using Latin hypercube sampling. *Hydrological Processes*, *27*(18), 2666–2675. https://doi.org/10.1002/hyp.9386

Foster, L. M., Williams, K. H., & Maxwell, R. M. (2020). Resolution matters when modeling climate change in headwaters of the Colorado River. *Environmental Research Letters*. https://doi.org/10.1088/1748-9326/aba77f

Gates WL (1992) AMIP: the atmospheric model intercomparison project. Bull Am Meteorol Soc 73(12):1962–1970. doi:10.1175/1520-0477(1992)073<1962:ATAMIP>2.0.CO;2

Geologic Map of California, 2015. Geologic Map of California [WWW Document]. Geologic Map of California. URL https://maps.conservation.ca.gov/cgs/gmc/ (accessed 10.17.18).

Gent, P. R., Danabasoglu, G., Donner, L. J., Holland, M. M., Hunke, E. C., Jayne, S. R., et al. (2011). The Community Climate System Model Version 4. *Journal of Climate*, *24*(19), 4973–4991. https://doi.org/10.1175/2011JCLI4083.1

Gershunov, A., Shulgina, T., Clemesha, R.E.S. et al. (2019). Precipitation regime change in Western North America: The role of Atmospheric Rivers. Sci Rep 9, 9944. https://doi.org/10.1038/s41598-019-46169-w

Gettelman, A., and Morrison, H. (2015). Advanced Two-Moment Bulk Microphysics for Global Models. Part I: Off-Line Tests and Comparison with Other Schemes. Journal of Climate 28, 3, 1268-1287. https://doi.org/10.1175/JCLI-D-14-00102.1

Gilbert, J.M., Maxwell, R.M., 2017. Examining regional groundwater - surface water dynamics using an integrated hydrologic model of the San Joaquin River basin. Hydrology and Earth System Sciences 21, 923–947. https://doi.org/10.5194/hess-21-923-2017

1227 Gleick, P. H. (1987). The development and testing of a water balance model for climate impact
1228 assessment: Modeling the Sacramento Basin. *Water Resources Research*, *23*(6), 1049–
1229 1061. https://doi.org/10.1029/WR023i006p01049
1230 Godsey, S. E., Kirchner, J. W., & Tague, C. L. (2014). Effects of changes in winter snowpacks on
1231 summer low flows: case studies in the Sierra Nevada, California, USA. *Hydrological*
1232 *Processes*, *28*(19), 5048–5064. https://doi.org/10.1002/hyp.9943
1233 Griffin, D., & Anchukaitis, K. J. (2014). How unusual is the 2012–2014 California drought?
1234 *Geophysical Research Letters*, *41*(24), 9017–9023.
1235 https://doi.org/10.1002/2014GL062433
1236 Haarsma, R. J., Roberts, M. J., Vidale, P. L., Senior, C. A., Bellucci, A., Bao, Q., Chang, P., Corti,
1237 S., Fučkar, N. S., Guemas, V., von Hardenberg, J., Hazeleger, W., Kodama, C., Koenigk,
1238 T., Leung, L. R., Lu, J., Luo, J.-J., Mao, J., Mizielinski, M. S., Mizuta, R., Nobre, P., Satoh,
1239 M., Scoccimarro, E., Semmler, T., Small, J., and von Storch, J.-S. (2016). High Resolution
1240 Model Intercomparison Project (HighResMIP v1.0) for CMIP6, Geosci. Model Dev., 9,
1241 4185–4208, https://doi.org/10.5194/gmd-9-4185-2016.
1242 Harbaugh AW (2005) MODFLOW-2005, The U.S. Geological Survey modular ground-water
1243 model: the ground-water flow process. US Geol Surv Tech Methods 6-
1244 A16. http://pubs.usgs.gov/tm/2005/tm6A16/.
1245 Harpold, A. A., & Molotch, N. P. (2015). Sensitivity of soil water availability to changing
1246 snowmelt timing in the western U.S. *Geophysical Research Letters*, *42*(19), 8011–8020.
1247 https://doi.org/10.1002/2015GL065855
1248 Hayhoe, K., Cayan, D., Field, C. B., Frumhoff, P. C., Maurer, E. P., Miller, N. L., et al. (2004).
1249 Emissions pathways, climate change, and impacts on California. *Proceedings of the*

National Academy of Sciences, *101*(34), 12422–12427. https://doi.org/10.1073/pnas.0404500101

He, M., Anderson, M., Schwarz, A., Das, T., Lynn, E., Anderson, J., et al. (2019). Potential Changes in Runoff of California's Major Water Supply Watersheds in the 21st Century. *Water*, *11*(8), 1651. https://doi.org/10.3390/w11081651

Herrington, A. R., P. H. Lauritzen, M. A. Taylor, S. Goldhaber, B. E. Eaton, J. T. Bacmeister, K. A. Reed, and P. A. Ullrich (2019). Physics–Dynamics Coupling with Element-Based High-Order Galerkin Methods: Quasi-Equal-Area Physics Grid. Mon. Wea. Rev., 147, 69–84, https://doi.org/10.1175/MWR-D-18-0136.1.

Homer, C., Dewitz, J., Yang, L., Jin, S., Danielson, P., Xian, G., et al. (2015). Completion of the 2011 National Land Cover Database for the conterminous United States–representing a decade of land cover change information. *Photogrammetric Engineering & Remote Sensing*, *81*(5), 345–354.

Huang, X., Rhoades, A. M., Ullrich, P. A., & Zarzycki, C. M. (2016). An evaluation of the variable-resolution CESM for modeling California's climate. *Journal of Advances in Modeling Earth Systems*, *8*(1), 345–369. https://doi.org/10.1002/2015MS000559

Huang, X., Stevenson, S., & Hall, A. D. (2020). Future warming and intensification of precipitation extremes: A "double whammy" leading to increasing flood risk in California. Geophysical Research Letters, 47, e2020GL088679. https://doi.org/10.1029/2020GL088679

Hurrell, J. W., Holland, M. M., Gent, P. R., Ghan, S., Kay, J. E., Kushner, P. J., et al. (2013). The Community Earth System Model: A Framework for Collaborative Research. *Bulletin of*

the American Meteorological Society, *94*(9), 1339–1360. https://doi.org/10.1175/BAMS-D-12-00121.1

Jones, P. W., (1999). First- and Second-Order Conservative Remapping Schemes for Grids in Spherical Coordinates. Mon. Wea. Rev., 127, 2204–2210, https://doi.org/10.1175/1520-0493(1999)127<2204:FASOCR>2.0.CO;2.

IGBP, 2018. Global plant database published - IGBP [WWW Document]. URL http://www.igbp.net/news/news/news/globalplantdatabasepublished.5.1b8ae20512db692f2a6800014762.html (accessed 10.17.18).

Jennings, C. W., Strand, R. G., & Rogers, T. H. (1977). Geologic map of California. Sacramento, Calif.: Division of Mines and Geology.

Kampenhout, L. van, Rhoades, A. M., Herrington, A. R., Zarzycki, C. M., Lenaerts, J. T. M., Sacks, W. J., & Broeke, M. R. van den. (2019). Regional grid refinement in an Earth system model: impacts on the simulated Greenland surface mass balance. *The Cryosphere*, *13*(6), 1547–1564. https://doi.org/10.5194/tc-13-1547-2019

Kollet, S. J., & Maxwell, R. M. (2006). Integrated surface–groundwater flow modeling: A free-surface overland flow boundary condition in a parallel groundwater flow model. *Advances in Water Resources*, *29*(7), 945–958. https://doi.org/10.1016/j.advwatres.2005.08.006

Lemordant, L., Gentine, P., Swann, A. S., Cook, B. I., & Scheff, J. (2018). Critical impact of vegetation physiology on the continental hydrologic cycle in response to increasing CO2. *Proceedings of the National Academy of Sciences*, *115*(16), 4093–4098. https://doi.org/10.1073/pnas.1720712115

Liang, X., D. P. Lettenmaier, E. F. Wood, and S. J. Burges (1994), A simple hydrologically based model of land surface water and energy fluxes for general circulation models, J. Geophys. Res., 99(D7), 14415–14428, doi:10.1029/94JD00483.

Lundquist, J. D., Hughes, M., Henn, B., Gutmann, E. D., Livneh, B., Dozier, J., & Neiman, P. (2015). High-Elevation Precipitation Patterns: Using Snow Measurements to Assess Daily Gridded Datasets across the Sierra Nevada, California, Journal of Hydrometeorology, 16(4), 1773-1792. doi: https://journals.ametsoc.org/view/journals/hydr/16/4/jhm-d-15-0019_1.xml

Maina, Fadji Z., Siirila-Woodburn, E. R., Newcomer, M., Xu, Z., & Steefel, C. (2020a). Determining the impact of a severe dry to wet transition on watershed hydrodynamics in California, USA with an integrated hydrologic model. *Journal of Hydrology*, *580*, 124358. https://doi.org/10.1016/j.jhydrol.2019.124358

Maina, F. Z., Siirila-Woodburn, E. R., & Vahmani, P. (2020b). Sensitivity of meteorological-forcing resolution on hydrologic variables. *Hydrology and Earth System Sciences*, *24*(7), 3451–3474. https://doi.org/10.5194/hess-24-3451-2020

Maina, Fadji Zaouna, & Siirila-Woodburn, E. R. (2020c). Watersheds dynamics following wildfires: Nonlinear feedbacks and implications on hydrologic responses. *Hydrological Processes*, *34*(1), 33–50. https://doi.org/10.1002/hyp.13568

Mallakpour, I., Sadegh, M., AghaKouchak, A., 2018. A new normal for streamflow in California in a warming climate: Wetter wet seasons and drier dry seasons. Journal of Hydrology 567, 203–211. https://doi.org/10.1016/j.jhydrol.2018.10.023

Maurer, E. P. (2007). Uncertainty in hydrologic impacts of climate change in the Sierra Nevada, California, under two emissions scenarios. Climatic Change, 82(3), 309–325. https://doi.org/10.1007/s10584-006-9180-9

Maurer, E. P., & Duffy, P. B. (2005). Uncertainty in projections of streamflow changes due to climate change in California. Geophysical Research Letters, 32(3). https://doi.org/10.1029/2004GL021462

Maxwell, R. M. (2013). A terrain-following grid transform and preconditioner for parallel, large-scale, integrated hydrologic modeling. *Advances in Water Resources*, *53*, 109–117. https://doi.org/10.1016/j.advwatres.2012.10.001

Maxwell, R. M., & Condon, L. E. (2016). Connections between groundwater flow and transpiration partitioning. *Science*, *353*(6297), 377–380. https://doi.org/10.1126/science.aaf7891

Maxwell, R. M., & Miller, N. L. (2005). Development of a Coupled Land Surface and Groundwater Model. *Journal of Hydrometeorology*, *6*(3), 233–247. https://doi.org/10.1175/JHM422.1

Mayer, T. D., & Naman, S. W. (2011). Streamflow Response to Climate as Influenced by Geology and Elevation1. JAWRA Journal of the American Water Resources Association, 47(4), 724–738. https://doi.org/10.1111/j.1752-1688.2011.00537.xBoryan, C., Yang, Z., Mueller, R., Craig, M., 2011. Monitoring US agriculture: the US Department of Agriculture, National Agricultural Statistics Service, Cropland Data Layer Program. Geocarto International 26, 341–358. https://doi.org/10.1080/10106049.2011.562309

Mallakpour, I., Sadegh, M., AghaKouchak, A., 2018. A new normal for streamflow in California in a warming climate: Wetter wet seasons and drier dry seasons. Journal of Hydrology 567, 203–211. https://doi.org/10.1016/j.jhydrol.2018.10.023

Maxwell, R.M., 2013. A terrain-following grid transform and preconditioner for parallel, large-scale, integrated hydrologic modeling. Advances in Water Resources 53, 109–117. https://doi.org/10.1016/j.advwatres.2012.10.001

McEvoy, D.J., Pierce, D.W., Kalansky, J.F., Cayan, D.R., Abatzoglou, J.T., 2020. Projected Changes in Reference Evapotranspiration in California and Nevada: Implications for Drought and Wildland Fire Danger. Earth's Future 8, e2020EF001736. https://doi.org/10.1029/2020EF001736

Milly, P. C. D., & Dunne, K. A. (2017). A Hydrologic Drying Bias in Water-Resource Impact Analyses of Anthropogenic Climate Change. *JAWRA Journal of the American Water Resources Association*, *53*(4), 822–838. https://doi.org/10.1111/1752-1688.12538

Milly, P. C. D., Dunne, K. A., & Vecchia, A. V. (2005). Global pattern of trends in streamflow and water availability in a changing climate. *Nature*, *438*(7066), 347–350. https://doi.org/10.1038/nature04312

Mote, P. W., Hamlet, A. F., Clark, M. P., & Lettenmaier, D. P. (2005). Declining mountain snowpack in western north america*. *Bulletin of the American Meteorological Society*, *86*(1), 39–50. https://doi.org/10.1175/BAMS-86-1-39

Musselman, K. N., Clark, M. P., Liu, C., Ikeda, K., & Rasmussen, R. (2017). Slower snowmelt in a warmer world. *Nature Climate Change*, *7*(3), 214–219. https://doi.org/10.1038/nclimate3225

1357 Musselman, K. N., Molotch, N. P., & Margulis, S. A. (2017). Snowmelt response to simulated
1358 warming across a large elevation gradient, southern Sierra Nevada, California. *The*
1359 *Cryosphere*, *11*(6), 2847–2866. https://doi.org/10.5194/tc-11-2847-2017
1360 National Operational Hydrologic Remote Sensing Center. (2004). Snow Data Assimilation
1361 System (SNODAS) Data Products at NSIDC. https://doi.org/10.7265/N5TB14TC.
1362 Neelin, J. D., Langenbrunner, B., Meyerson, J. E., Hall, A., & Berg, N. (2013). California Winter
1363 Precipitation Change under Global Warming in the Coupled Model Intercomparison
1364 Project Phase 5 Ensemble. Journal of Climate, 26(17), 6238–6256.
1365 https://doi.org/10.1175/JCLI-D-12-00514.1
1366 Neitsch, S. L., Arnold, J. G., Kiniry, J. R., & Williams, J. R. (2001). Soil and Water Assessment
1367 tool (SWAT) user's manual version 2000. Grassland Soil and Water Research Laboratory.
1368 Temple, TX: ARS.
1369 Niraula, R., Meixner, T., Dominguez, F., Bhattarai, N., Rodell, M., Ajami, H., et al. (2017). How
1370 Might Recharge Change Under Projected Climate Change in the Western U.S.?
1371 *Geophysical Research Letters*, *44*(20), 10,407-10,418.
1372 https://doi.org/10.1002/2017GL075421
1373 Niu, G.-Y., et al. (2011), The community Noah land surface model with multiparameterization
1374 options (Noah-MP): 1. Model description and evaluation with local-scale measurements. J.
1375 Geophys. Res., 116, D12109, doi: 10.1029/2010JD015139.
1376 SMAP. (2015). Soil Moisture Active Passive. Retrieved October 18, 2018, from SMAP
1377 website: https://smap.jpl.nasa.gov/
1378 Siirila-Woodburn, E. R., Rhoades, A. M., Hatchett, B. J., Huning, L. S., Szinai, J., Tague, C., Nico,
1379 P. S., Feldman, D. R., Jones, A. D., Collins, W. D., and Kaatz, L.: A low-to-no snow future

and its impacts on water resources in the western United States, Nature Reviews Earth and Environment, https://doi.org/10.1038/s43017-021-00219-y, 2021.

Pascolini-Campbell, M., Reager, J. T., Chandanpurkar, H. A., & Rodell, M. (2021). A 10 per cent increase in global land evapotranspiration from 2003 to 2019. Nature, 593(7860), 543–547. https://doi.org/10.1038/s41586-021-03503-5

Payne, A. E., Demory, M.-E., Leung, L. R., Ramos, A. M., Shields, C. A., Rutz, J. J., et al. (2020). Responses and impacts of atmospheric rivers to climate change. *Nature Reviews Earth & Environment*, *1*(3), 143–157. https://doi.org/10.1038/s43017-020-0030-5

Persad, G. G., Swain, D. L., Kouba, C., & Ortiz-Partida, J. P. (2020). Inter-model agreement on projected shifts in California hydroclimate characteristics critical to water management. Climatic Change, 162(3), 1493–1513. https://doi.org/10.1007/s10584-020-02882-4

Ralph, F. M., & Dettinger, M. D. (2011). Storms, floods, and the science of atmospheric rivers. *Eos, Transactions American Geophysical Union*, *92*(32), 265–266. https://doi.org/10.1029/2011EO320001

Ralph, F. Martin, Neiman, P. J., Wick, G. A., Gutman, S. I., Dettinger, M. D., Cayan, D. R., & White, A. B. (2006). Flooding on California's Russian River: Role of atmospheric rivers. *Geophysical Research Letters*, *33*(13). https://doi.org/10.1029/2006GL026689

Rasmussen, R., Liu, C., Ikeda, K., Gochis, D., Yates, D., Chen, F., et al. (2011). High-Resolution Coupled Climate Runoff Simulations of Seasonal Snowfall over Colorado: A Process Study of Current and Warmer Climate. *Journal of Climate*, *24*(12), 3015–3048. https://doi.org/10.1175/2010JCLI3985.1

Rhoades, A. M., Huang, X., Ullrich, P. A., & Zarzycki, C. M. (2016). Characterizing Sierra Nevada Snowpack Using Variable-Resolution CESM. *Journal of Applied Meteorology and Climatology*, *55*(1), 173–196. https://doi.org/10.1175/JAMC-D-15-0156.1

Rhoades, A. M., Ullrich, P. A., & Zarzycki, C. M. (2018a). Projecting 21st century snowpack trends in western USA mountains using variable-resolution CESM. *Climate Dynamics*, *50*(1), 261–288. https://doi.org/10.1007/s00382-017-3606-0

Rhoades, A. M., Jones, A. D., & Ullrich, P. A. (2018b). The changing character of the California Sierra Nevada as a natural reservoir. Geophysical Research Letters, 45, 13,008– 13,019. https://doi.org/10.1029/2018GL080308

Rhoades, A. M., Ullrich, P. A., Zarzycki, C. M., Johansen, H., Margulis, S. A., Morrison, H., et al. (2018c). Sensitivity of Mountain Hydroclimate Simulations in Variable-Resolution CESM to Microphysics and Horizontal Resolution. *Journal of Advances in Modeling Earth Systems*, *10*(6), 1357–1380. https://doi.org/10.1029/2018MS001326

Rhoades, A. M., Jones, A. D., O'Brien, T. A., O'Brien, J. P., Ullrich, P. A., & Zarzycki, C. M. (2020a). Influences of North Pacific Ocean domain extent on the western U.S. winter hydroclimatology in variable-resolution CESM. Journal of Geophysical Research: Atmospheres, 125, e2019JD031977. https://doi.org/10.1029/2019JD031977

Rhoades, A. M., Jones, A. D., Srivastava, A., Huang, H., O'Brien, T. A., Patricola, C. M., et al. (2020b). The shifting scales of western U.S. landfalling atmospheric rivers under climate change. Geophysical Research Letters, 47, e2020GL089096. https://doi.org/10.1029/2020GL089096

Rhoades, A. M., Risser, M. D., Stone, D. A., Wehner, M. F., & Jones, A. D. (2021). Implications of warming on western United States landfalling atmospheric rivers and their flood

damages. Weather and Climate Extremes, 32, 100326, https://doi.org/10.1016/j.wace.2021.100326

Richards, L. A. (1931). Capillary conduction of liquids through porous medium. *Journal of Applied Physics*, *1*(5), 318–333. https://doi.org/10.1063/1.1745010

Safeeq, M., Grant, G. E., Lewis, S. L., Kramer, M. G., & Staab, B. (2014). A hydrogeologic framework for characterizing summer streamflow sensitivity to climate warming in the Pacific Northwest, USA. *Hydrology and Earth System Sciences*, (18), 1–8. https://doi.org/10.5194/hess-18-3693-2014

Safeeq, M., Grant, G.E., Lewis, S.L. and Tague, C.L. (2013), Coupling snowpack and groundwater dynamics to interpret historical streamflow trends in the western United States. Hydrol. Process., 27: 655-668. https://doi.org/10.1002/hyp.9628

Safeeq, Mohammad, Grant, G. E., Lewis, S. L., & Staab, B. (2015). Predicting landscape sensitivity to present and future floods in the Pacific Northwest, USA. *Hydrological Processes*, *29*(26), 5337–5353. https://doi.org/10.1002/hyp.10553

SCRIPPS Institution of Oceanograohy. (2017, April). Northern California Just Surpassed the Wettest Year on Record | Scripps Institution of Oceanography, UC San Diego. Retrieved from https://scripps.ucsd.edu/news/northern-california-just-surpassed-wettest-year-record

Shukla, S., Safeeq, M., AghaKouchak, A., Guan, K., & Funk, C. (2015). Temperature impacts on the WY 2014 drought in California. *Geophysical Research Letters*, 4384–4393. https://doi.org/10.1002/2015GL063666@10.1002/(ISSN)1944-8007.CALDROUGHT1

Son, K., & Tague, C. (2019). Hydrologic responses to climate warming for a snow-dominated watershed and a transient snow watershed in the California Sierra. *Ecohydrology*, *12*(1), e2053. https://doi.org/10.1002/eco.2053

1447 Strachan, S., and Daly, C. (2017), Testing the daily PRISM air temperature model on semiarid
1448 mountain slopes, J. Geophys. Res. Atmos., 122, 5697– 5715, doi:10.1002/2016JD025920.
1449 Swain, D. L., Langenbrunner, B., Neelin, J. D., & Hall, A. (2018). Increasing precipitation
1450 volatility in twenty-first-century California. *Nature Climate Change*, *8*(5), 427–433.
1451 https://doi.org/10.1038/s41558-018-0140-y
1452 Tague, C., & Peng, H. (2013). The sensitivity of forest water use to the timing of precipitation and
1453 snowmelt recharge in the California Sierra: Implications for a warming climate. *Journal of*
1454 *Geophysical Research: Biogeosciences*, *118*(2), 875–887.
1455 https://doi.org/10.1002/jgrg.20073
1456 Tang, G., Li, S., Yang, M., Xu, Z., Liu, Y., & Gu, H. (2019). Streamflow response to snow regime
1457 shift associated with climate variability in four mountain watersheds in the US Great Basin.
1458 *Journal of Hydrology*, *573*, 255–266. https://doi.org/10.1016/j.jhydrol.2019.03.021
1459 The NCAR Command Language (Version 6.6.2) (2021). Boulder, Colorado:
1460 UCAR/NCAR/CISL/TDD, 851 http://dx.doi.org/10.5065/D6WD3XH5.
1461 Trefry, M.G.; Muffels, C. (2007). "FEFLOW: a finite-element ground water flow and transport
1462 modeling tool". Ground Water. 45 (5): 525–528. doi:10.1111/j.1745-6584.2007.00358.x
1463 Vicuna, S., & Dracup, J. A. (2007). The evolution of climate change impact studies on hydrology
1464 and water resources in California. *Climatic Change*, *82*(3), 327–350.
1465 https://doi.org/10.1007/s10584-006-9207-2
1466 Vicuna, Sebastian, Maurer, E. P., Joyce, B., Dracup, J. A., & Purkey, D. (2007). The Sensitivity
1467 of California Water Resources to Climate Change Scenarios1. *JAWRA Journal of the*
1468 *American Water Resources Association*, *43*(2), 482–498. https://doi.org/10.1111/j.1752-
1469 1688.2007.00038.x

Wang, S.-Y. S., Yoon, J.-H., Becker, E., & Gillies, R. (2017). California from drought to deluge. Nature Climate Change, 7(7), 465. https://doi.org/10.1038/nclimate3330

Welch, L.A., Allen, D.M., 2014. Hydraulic conductivity characteristics in mountains and implications for conceptualizing bedrock groundwater flow. Hydrogeol J 22, 1003–1026. https://doi.org/10.1007/s10040-014-1121-5

Wu, C., Liu, X., Lin, Z., Rhoades, A. M., Ullrich, P. A., Zarzycki, C. M., et al. (2017). Exploring a Variable-Resolution Approach for Simulating Regional Climate in the Rocky Mountain Region Using the VR-CESM. *Journal of Geophysical Research: Atmospheres*, *122*(20), 10,939-10,965. https://doi.org/10.1002/2017JD027008

Zarzycki, C. M., Levy, M. N., Jablonowski, C., Overfelt, J. R., Taylor, M. A., and Ullrich, P. A. (2014). Aquaplanet Experiments Using CAM's Variable-Resolution Dynamical Core. Journal of Climate 27, 14, 5481-5503, https://doi.org/10.1175/JCLI-D-14-00004.1